Q. J. R. Meteorol. Soc. (1996), **122**, pp. 451–482

The effect on regional and global climate of expansion of the world's deserts

By PAUL A. DIRMEYER* and J. SHUKLA
Center for Ocean–Land–Atmosphere Studies, USA

(Received 18 June 1994; revised 27 June 1995)

SUMMARY

An atmospheric general-circulation model with realistic land-surface properties is used to investigate the climatic effect of doubling the extent of the earth's deserts. Control and anomaly integrations are performed for 10 years. In the anomaly case, deserts are expanded over northern and southern Africa, Australia, south-central Asia, south-western North America, and parts of South America.

In the anomaly case, the troposphere is cooler across most of the tropics and subtropics, including all areas where desertification occurs. Remote effects in the winter circulation include a pronounced trough over northern Europe, and increased geopotential heights over the southern oceans. The response of climate in deforested areas is not uniform between the regions. The magnitude and seasonality of the changes, particularly in precipitation, seem to be functions of the monsoon regime. Northern Africa suffers a strong year-round drought, suggesting this area is most sensitive to desertification, and southern Africa has a somewhat weaker year-round drought. Rainfall over desertified parts of Asia, Australia and western South America decreases only during the summer, and not during the winter. North America and the Nordeste region of Brazil show the least sensitivity to desertification. Most regions show a notable correlation between decreases in evapotranspiration and resulting precipitation. However, regional land–sea distributions in the vicinity of each desertified area appear to determine the sensitivity and response of the local climate via induced changes in moisture flux convergence. Thus, different regions exhibit different responses of climate to desertification. Surface temperature decreases over most desertified areas, owing to reduced absorption of short-wave radiation by the brighter surface. Some regions, particularly the Sahel, show an increase in surface temperature caused by decreased soil moisture and latent-heat flux.

KEYWORDS: Climate change Climate modelling Desertification Regional climate sensitivity

1. INTRODUCTION

Charney (1975) was among the first to investigate the potential effect on climate of changes in vegetation cover in desert margins. He concluded that changes in net surface albedo directly affect the surface energy balance. In semi-arid regions, an increase in albedo leads to a loss of radiative energy from the surface, and convective overturning is reduced (Charney *et al.* 1977; Chervin 1979). As a result, precipitation decreases. The ensuing reduction in vegetation cover could further enhance the albedo increase, establishing a positive feedback (Dickinson and Hanson 1984).

Changes in surface roughness affect the balance of momentum at the surface, and can affect the efficiency of the transport of heat and moisture between land and air. Studies of reductions of roughness length over desert show that precipitation decreases unless moisture convergence is already small (Sud and Smith 1985a). Over other land areas, reductions in roughness change rainfall patterns unsystematically, by altering the distribution of low-level convergence (Sud and Smith 1985b; Sud *et al.* 1988).

Soil moisture interacts with the atmosphere via evapotranspiration, affecting the surface moisture and energy balances. Soil moisture has been found to have a positive correlation on precipitation in semi-arid regions (Namias 1959, 1960). Modelling studies generally confirm the positive correlation between evapotranspiration and rainfall (Rind 1982; Shukla and Mintz 1982; Mintz 1984; Oglesby and Erickson 1989). However, Sud and Fennessy (1984) found precipitation to increase over arid regions when evaporation was decreased.

Changes in the biosphere affect all three of these properties. Vegetation controls transpiration and thus the transport of moisture from soil to atmosphere. The presence and

* Corresponding author: Center for Ocean–Land–Atmosphere Studies, 4041 Powder Mill Road, Suite 302, Calverton, Maryland 20705-3106, USA.

density of foliage alter radiation and momentum transfer (Dickinson 1983). Plant canopies act to insulate the ground, mediating temperature at the surface, partially decoupling the soil from the free atmosphere (Schwartz and Karl 1990). Desertification can be expected to increase surface albedo while decreasing surface roughness. Both of these changes can reduce latent-heat flux from the surface, as can the loss of transpiration from the reduced vegetation mass. However, reduced rainfall as postulated by Charney *et al.* (1977) and degradation of soils can overcome the reduction in evapotranspiration to cause a net decrease in soil moisture. Since all soil moisture must originate as rainfall, the change in precipitation is critical to the fate of soil moisture. Decreased albedo and roughness may also be expected to decrease sensible-heat flux from the surface.

There is a great deal of observational evidence that desertification has been occurring over much of the world for the last several decades. Skoupy (1987) documents the degradation of vegetation in sub-Sahara Africa over the last half-century. Pittock (1983) and Allan and Haylock (1993) describe the decrease in rainfall observed over parts of Australia since the 1940s. McNeill *et al.* (1994) describe the effects of agriculturally induced degradation in marginal vegetated areas at several locations around the world. Graetz (1994) reports on the loss of grasslands to desertification, calling the transformation much more serious and widespread than the loss of grasslands converted to croplands. Forest clearing can also lead to serious degradation (Williams 1990, 1994). The degree of desertification on each continent, with differing contexts and definitions, has been published in several reports (Dregne 1983; Mabbutt 1984; World Resources Institute (WRI) 1992). Table 1 shows the percentage of land in Africa, Asia, Australia, North and South America which is defined as arid (encompassing both arid and semi-arid steppe vegetation) by Drenge (1983), rangeland by Mabbutt (1984), or in human use by WRI (1992), as well as the percentage of those lands which have suffered desertification due to various factors. WRI (1992) focuses on soil degradation, while the other studies consider effects on vegetation and productivity. Due to lack of availability of data in many parts of the world, particularly in developing nations, there is some uncertainty and discrepancy amongst the studies. Intensification of deserts is seen to be extensive on all of the continents examined: about half of the arid lands, principally the marginal semi-arid regions, have experienced at least moderate desertification. Halpern (1993) estimates that 70% of drylands are affected by desertification, including 73% of rangeland and 47% of marginal farmland, affecting about one sixth of the world's population.

There are several potential causes of desertification. Expansion of deserts can be due to poor land management and destructive land-use practices (Dregne 1983; Skoupy 1987). Desertification may be caused by the warming and drying of continents predicted by some to accompany the increase of carbon dioxide in the atmosphere (Manabe *et al.* 1981, 1992; Washington and Meehl 1984; Bolin *et al.* 1986). On the other hand, expansion of deserts may be part of the natural variability of the climate system (Nicholson 1979), with possible links to variations in sea surface temperature (Lamb and Peppler 1992). It is quite possible that all three of these aspects play a role in the observed increase in desert area. However, we do not attempt to address the potential causes of desertification in this study.

General-circulation model (GCM) studies have examined desertification effects in various regions of the world. The effects of prolonged drought and desertification on the Sahel region of Africa have been modelled extensively. One of the first studies was by Charney *et al.* (1977), who examined the effect of albedo increase and extremes in evaporation. Sud and Fennessy (1982, 1984) examined the effects of albedo increase and reduced evaporation separately over northern Africa. Laval and Picon (1986) concentrated on the Sahel, where they increased albedo. Xue and Shukla (1993) changed vegetation types in a biosphere model to simulate the entire range of physical changes that accompany

TABLE 1. AREAS OF LANDS (%) AFFECTED BY DESERTIFICATION ON FIVE CONTINENTS

Drenge (1983)		Moderate/severe desertification	
	Continent that is arid	Arid land	Continent
Africa	57	28	16
Asia	36	49	17
Australia	83	56	52
North America	18	90	16
South America	17	56	10
Mabbutt (1984)		**Desertified**	
	Area that is rangeland	Rangeland	Continent
Africa	23	86	20
Asia	19	72	14
Australia	59	22	13
Anglo America	14	42	6
Latin America	12	72	9
WRI (1992)		**Desertified**	
	Continent in use	Used land	Continent
Africa	59	27	16
Asia	55	31	17
Australia	71	19	13
North America	43	15	6
South America	78	18	14

desertification. These studies all found precipitation to decrease as a result of simulated desertification. Sud and Molod (1988) concentrated on the effect of revegetating northern Africa by decreasing surface albedo and increasing soil moisture. Xue and Shukla (1995) have likewise examined afforestation in the Sahel using a more sophisticated biosphere model. Modelling studies have been performed for other parts of the world. Charney *et al.* (1977) and Sud and Fennessy (1982, 1984) also examined albedo and evaporation effects over semi-arid regions of India, North America, and the Nordeste of Brazil. The effects of albedo increase on the Asian monsoon have been studied by Meehl (1994). These studies concur that land changes analogous to desertification lead to local prolonged drought conditions.

This study is unique in that we use a sophisticated biosphere model at the lower boundary. Rather than simply altering single parameters such as albedo or roughness length, we change the distribution of vegetation types to represent expansion of desert as in Xue and Shukla (1993). However, in this study, changes are made on five continents, not just over the Sahel. We attempt to represent the hypothetical global expansion of deserts by doubling the extent of deserts by intrusion into the marginal semi-arid regions. In addition, we examine the global as well as regional climate changes that widespread desertification may produce. The large spatial scale of homogeneous changes makes this experiment more of a sensitivity study than a realistic simulation of current desertification. Nonetheless, the statistics presented above suggest that our simulation of desertification may not be an unrealistic representation of future extents if land practices continue apace.

Section 2 describes the atmospheric GCM, the biosphere model, and the design of the experiment. A description of the control-case climatology is given in section 3. Section 4 contains descriptions of the large-scale anomalies, while the particular effects of desertification in different regions are illustrated in section 5. Section 6 presents our hypothesis of the mechanisms involved in the variety of climate changes found for different parts of the world in our results. A summary is presented in section 7.

2. Description of the experiment

Control and doubled-desert experiments are conducted using the Center for Ocean–Land–Atmosphere Studies atmospheric general-circulation model with specified lower-boundary conditions over ocean and a biosphere model over land. The atmospheric GCM used is a research version of the National Meteorological Center (NMC) global spectral model described by Sela (1980) with modifications and boundary conditions as described by Kinter *et al.* (1988). The model is spectral, with rhomboidal truncation at wave number 15 (R–15), and is discretized into 18 vertical layers with sigma (p/p_s where p is pressure and p_s is surface pressure) as a vertical coordinate. Resolution is concentrated near the lower boundary, with four layers in the lowest 11% of the atmosphere. Subgrid-scale physical parametrizations are computed on a Gaussian grid with a resolution of approximately 7.5° longitude by 4.5° latitude. Complete annual and diurnal solar variations are included. Schneider and Kinter (1994) describe the current version of the model, as well as its climatology when integrated at this horizontal resolution.

The lower-boundary conditions for the GCM over land are supplied by the simplified version of the simple biosphere (SiB) model of Sellers *et al.* (1986) which is described by Xue *et al.* (1991), and referred to hereafter as SSiB. Initial ground temperature and soil moisture are computed using the soil temperature method of Delsol *et al.* (1971), and the soil moisture data of Willmott *et al.* (1985). The initialization procedures are as described by Kinter *et al.* (1988) except that soil moisture is allowed to vary freely after initialization. Over ocean, the integrations use the seasonally varying climatological sea surface temperatures of the Comprehensive Ocean–Atmosphere Data Set (Slutz *et al.* 1985). The GCM includes the radiation scheme of Harshvardhan *et al.* (1987), the short-wave transfer scheme described by Lacis and Hansen (1974) as modified by Davies (1982), and the long-wave scheme of Harshvardhan and Corsetti (1984). Boundary-layer fluxes are those of Miyakoda and Sirutis (1986). Vertical diffusion is based on the second-order closure model of Mellor and Yamada (1982). Convection and large-scale precipitation are computed using a modification of the scheme of Kuo (1965) as described by Sela (1980), and the shallow-convection scheme is that of Tiedke (1984). The GCM uses the interactive model-generated cloud scheme of Hou (1990), which is based on that of Slingo (1987).

On the Gaussian grid, the earth's surface is comprised of 1920 grid points, of which 624 are land. There are 13 different land surface types: 11 types of vegetation-covered land as well as bare soil (which comprise the 12 vegetation types of SSiB) and permanent ice. In the control case, 34 grid points are designated as bare soil, and 49 are shrubs with bare soil (arid steppe). For this experiment, we refer to both types as 'desert'. Figure 1(a) shows the distribution of these two surface types in the control case. In the double-desert case the number of desert grid points increases from 83 to 160. The number of grid points with bare soil is increased from 34 to 84. Most of the additional points are taken from adjacent steppe lands. Nonetheless, the number of steppe grid points is increased to 76 by expansion into adjacent areas. Table 2 quantifies the changes to the affected vegetation types and presents annual mean surface albedo and roughness length for comparison. Bare-soil albedo is high with respect to observations outside of the Sahara–Arabia region. It should be noted that

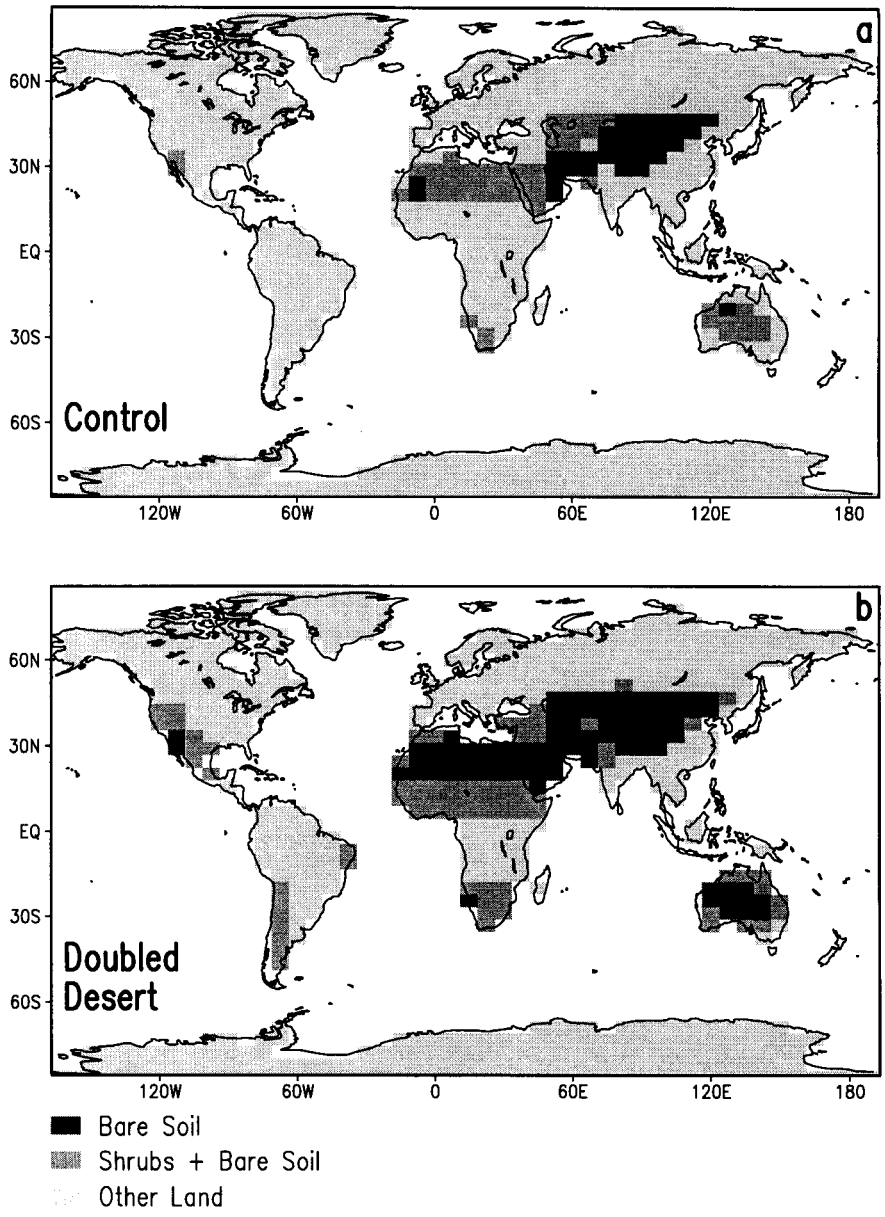

Figure 1. Location of bare soil and steppe vegetation (shrubs with bare soil) in (a) the control case and (b) the double-desert case.

changes in vegetation type result in changes to many parameters other than albedo and roughness length, but only those are shown here. More comprehensive descriptions of vegetation properties are given by Dorman and Sellers (1989) and Xue *et al.* (1991).

As shown in Fig. 1, desert is expanded on every ice-free continent except Europe. The core deserts are expanded, and surrounding regions are incorporated into the semi-arid steppe lands. The Sahara of Africa is intensified and the Sahel is pushed southward, similar to the experiment of Xue and Shukla (1993). The deserts of southern Africa are

TABLE 2. VEGETATION TYPES AFFECTED BY DESERTIFICATION, CHANGE IN THE NUMBER OF GRID POINTS, ANNUAL MEAN SHORT-WAVE SURFACE ALBEDO, AND ANNUAL RANGE OF ROUGHNESS LENGTH

Vegetation type	Change in number of points	Short-wave albedo	Roughness length (m)
Broad-leaf evergreen trees	−2	0.13	2.65
Broad-leaf deciduous trees	−1	0.13	0.52–1.04
Broad-leaf and needle-leaf trees	−1	0.13	0.54–0.57
Broad-leaf trees with ground cover	−27	0.20	0.73–0.97
Ground cover	−4	0.21	0.08
Broad-leaf shrubs with ground cover	−29	0.22	0.20–0.29
Broad-leaf deciduous trees over wheat cover	−13	0.17	0.14–0.52
Broad-leaf shrubs with bare soil*	+27	0.30	0.06–0.07
No vegetation*	+50	0.33	0.01

* 'Desert' type.

also expanded equatorward. The central desert of Australia is converted to bare soil, and much of the remaining continent is covered by steppe. Much of the bare soil of central Asia is in fact the rocky highland of the Himalayas. Deserts are intensified over Arabia, and expanded into the Middle East, Turkey, and the former Soviet republics of Asia. Desert is also expanded eastward in China, and Mongolia. In the western hemisphere, the deserts

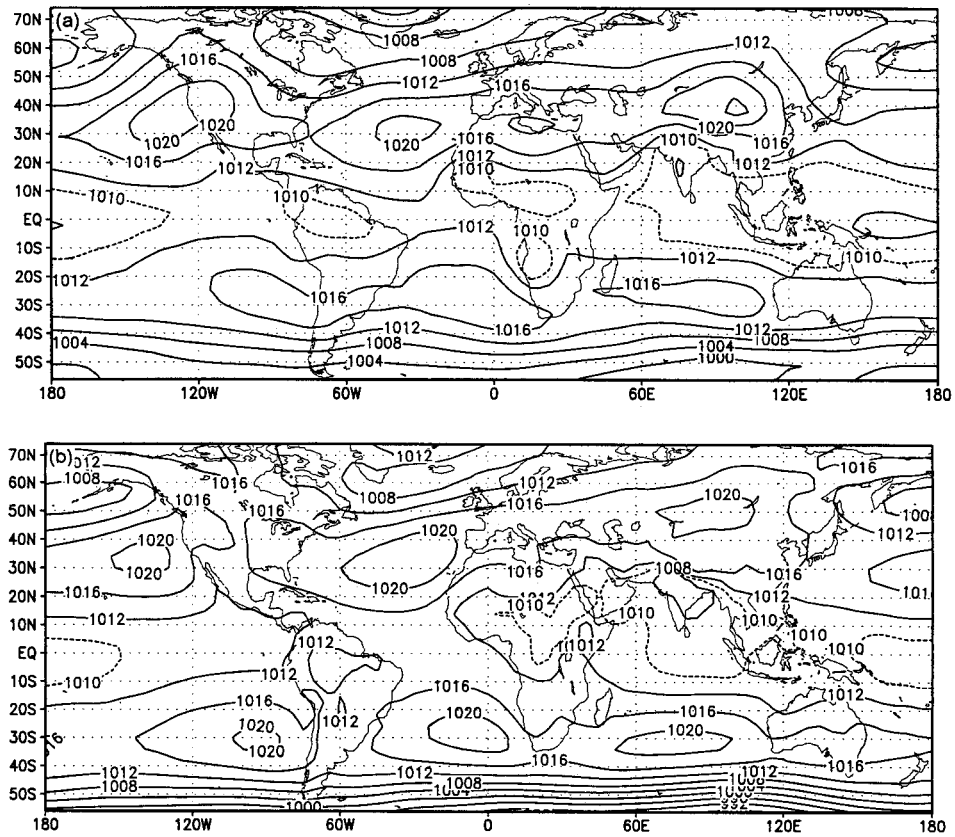

Figure 2. Time mean sea level pressure (mb) for (a) the last 8 years of the control case and (b) 13 years of ECMWF analyses (1980–92). The 1010 mb contour (dotted) is included over the tropics.

of the North American South-West are expanded in the United States and Mexico. The coastal deserts of western South America—too narrow to be resolved at R–15 resolution—are expanded, and the Nordeste of Brazil is converted to steppe.

Control and double-desert integrations are conducted for 10 years each. Initial conditions are taken from NMC analysis for 0000 GMT 1 December 1990. The model is first integrated for one month to allow some equilibration of the atmosphere toward the model climate. The integrations *per se* are considered to begin on 0000 GMT 1 January 1991. Since the integrations are 10 years in duration, the specific state of the initial condition can be considered unimportant in determining climatological features of the experiment. There is some evidence for climate drift in the model during the first 1–2 years, particularly in soil moisture. Time series of all fields show equilibration after year two. Therefore, only the last 8 years are used for statistical calculations.

3. Control integration

Even at the relatively low resolution, the GCM produces a very good climatology. Figure 2 shows the annual mean distribution of atmospheric mass, expressed as sea level pressure (SLP), from the control integration and the European Centre for Medium-Range Weather Forecasts (ECMWF) analyses for the period 1980–92. Although the zonal mean SLP in the tropics is slightly high compared with observations, the GCM simulates the

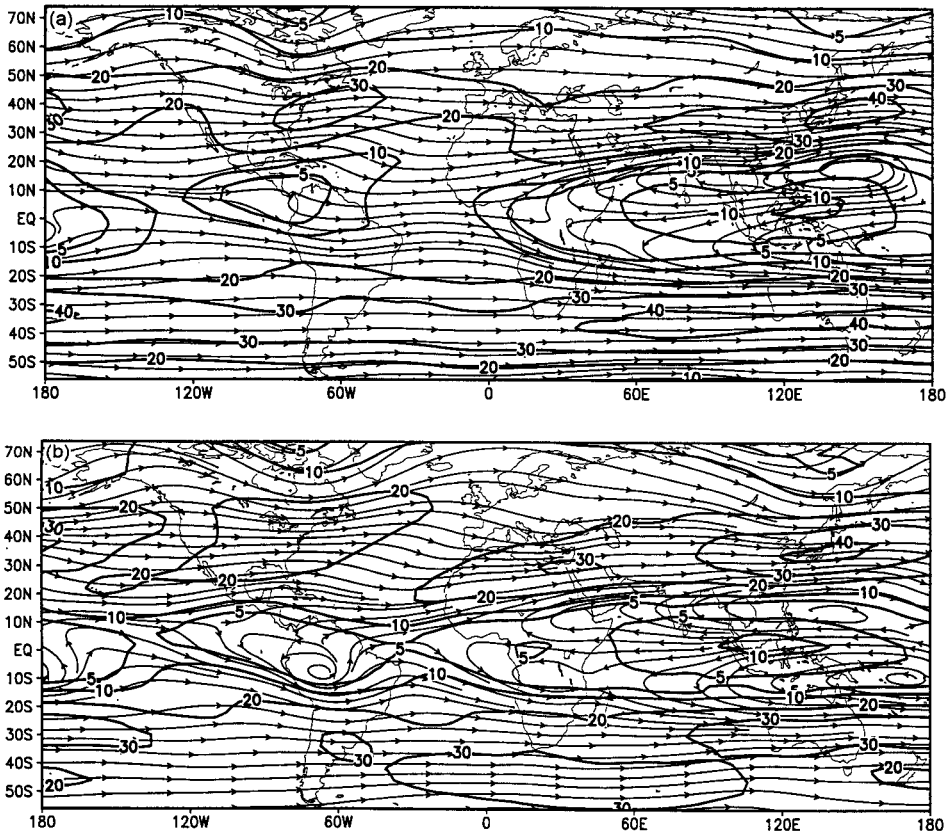

Figure 3. Time mean winds (m s^{-1}) at 200 mb for (a) the last 8 years of the control case and (b) 13 years of ECMWF analyses (1980–92).

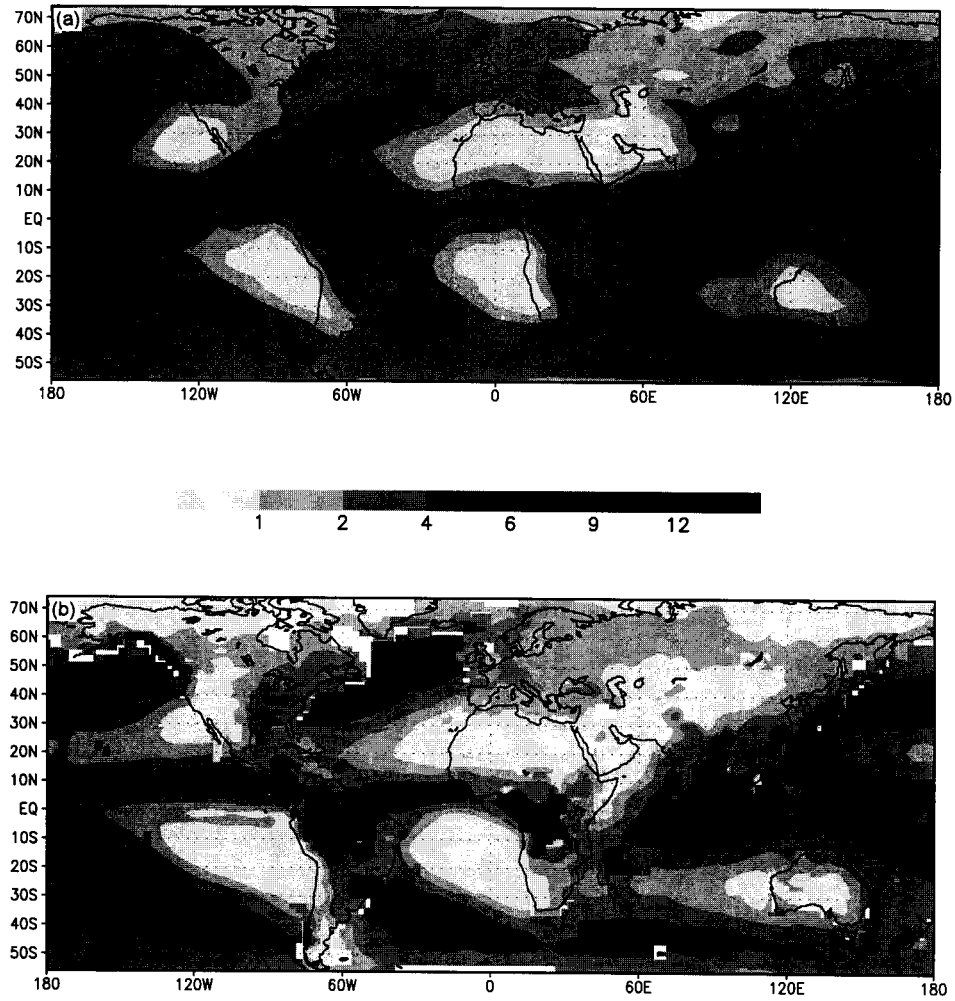

Figure 4. Time mean precipitation rate for (a) the last 8 years of the control case and (b) the composited station and satellite-derived observations (see text for description); and time mean precipitable water for (c) the last 8 years of the control case and (d) 13 years of ECMWF analyses (1980–92). Shading indicates rainfall rate in mm d^{-1} for (a) and (b) and mm of water for (c) and (d).

tropical trough, including the low-pressure centres over the Amazon, central Africa, India, and the western Pacific. The breaks in the trough over the tropical Atlantic and eastern Africa are also well simulated. The oceanic high-pressure centres in the subtropics are represented in both hemispheres, as is the Tibetan anticyclone. Pressure patterns in the mid latitudes are well depicted, especially in the northern hemisphere.

Figure 3 shows the annual mean 200 mb flow for the control integration and the ECMWF analyses. The circulation in the tropics is very well represented from the central Pacific westward to the east coast of Africa. The GCM produces excessive westerlies over the Atlantic, and underrepresents the easterly outflow from the Amazon basin. In the extratropics, the positions of the jet cores are well simulated in the northern hemisphere. However, the southern hemisphere jet is too narrow, and the jet cores in both hemispheres are too zonal and too strong. These errors are symptomatic of the deficiency in transient kinetic energy currently common to almost all GCMs.

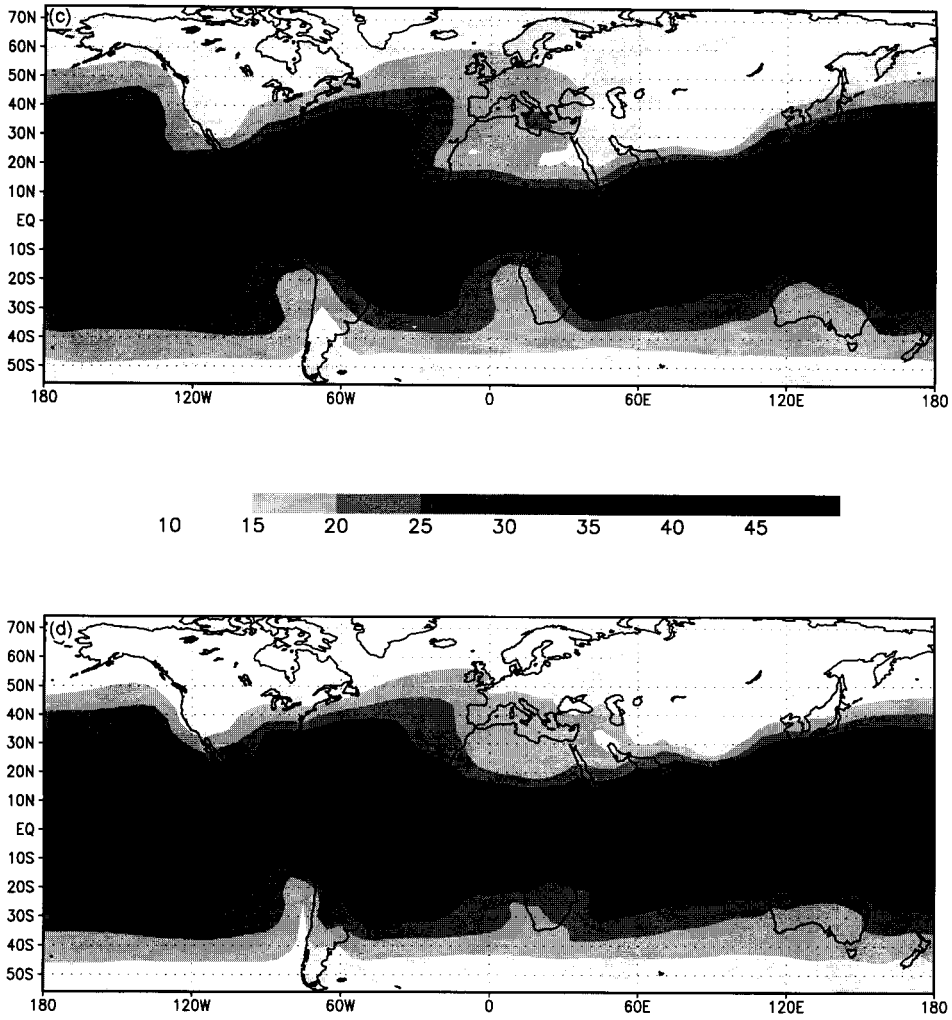

Figure 4. Continued.

Annual mean precipitation from the control integration is compared with a composite of observed precipitation based on *in situ* and satellite measurements in Figs. 4(a) and (b). The observed composite is prepared from 13 years (1979–91) of satellite-derived estimates over ocean of Spencer (1993), 15 years (1979–93) from the Climate Anomaly Monitoring System (CAMS) station precipitation data archive (Ropelewski *et al.* 1985) gridded over land, and 7 years (1986–92) of the Geostationary Operational Environment Satellite (GOES) precipitation index (GPI) estimates over the tropics (Janowiak and Arkin 1991). The Spencer data are used exclusively over the extratropical oceans, but GPI and Spencer data are averaged over oceans between 30°S and 30°N. GPI estimates are also used to fill gaps in the CAMS data over land in the tropics, and around coastlines where gaps exist due to the differing grids of the CAMS and Spencer data. No smoothing has been performed, so discontinuities may exist where different data sets abut.

The arid regions correlate well, except over the highlands of central Asia where the GCM is too wet. There is also good correspondence of rain bands in the tropics as well as

the mid latitudes. The model misses the precipitation maximum over the Bay of Bengal and Bangladesh. Also, maximum rainfall rates in the Inter-Tropical Convergence Zone (ITCZ) and South Pacific Convergence Zone are undersimulated. This is probably due to the inability of this low-resolution model to concentrate the ITCZ accurately. Nonetheless, the model does a good job of capturing the major climatological precipitation features. Figures 4(c) and (d) compare simulated annual mean precipitable water with ECMWF analyses for the period 1980–92. Both the meridional distribution and zonal assymetries of precipitable water are well simulated.

By comparing Figs. 1 and 4, one can see that regions of bare soil in the double-desert integration largely correspond to the land areas with precipitation of less than 1 mm d^{-1} in the composited data, and substantial potential evaporation. Steppes cover adjacent areas generally corresponding to areas with rainfall rates less than 2 mm d^{-1}. Some correspondence is lost in areas with steep precipitation gradients, such as the Sahel. Again, resolution of the model limits the accuracy in details. Nonetheless, our choice of regions for expanded desert do not appear unreasonable, assuming that existing vegetation is marginal and could be easily stressed by human activity or climate fluctuations.

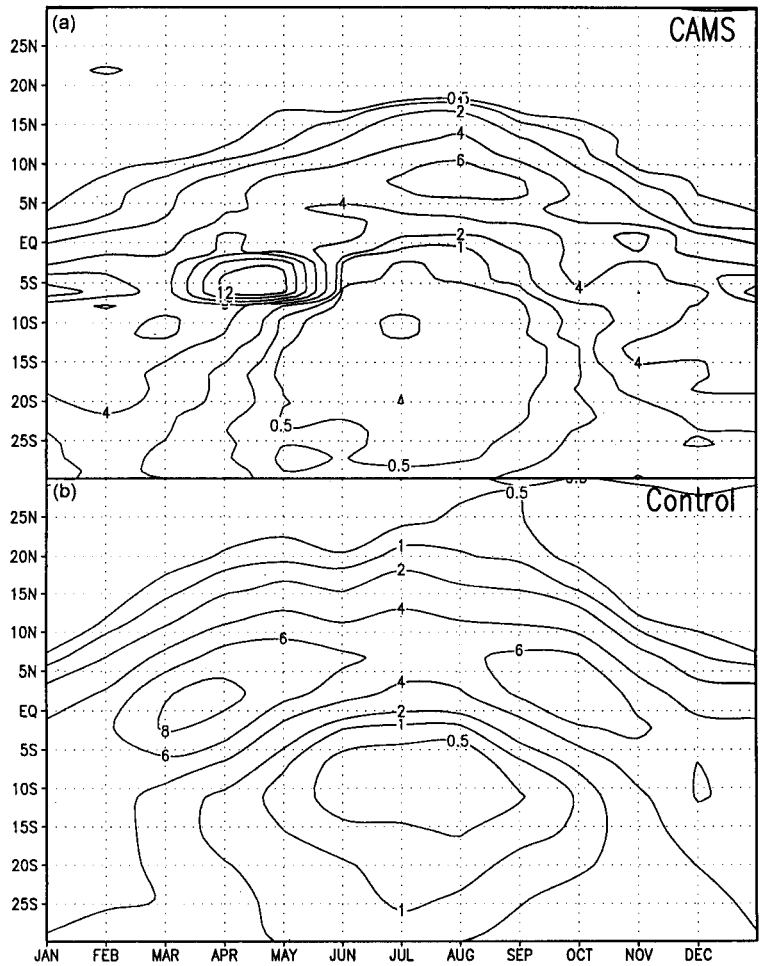

Figure 5. Mean annual cycle of climatological precipitation as a function of latitude averaged between 12°E and 42°E for (a) gridded CAMS station data and (b) the control case (see text). Units are mm d^{-1}.

The model simulation of the annual cycle of precipitation over central Africa is compared with the CAMS climatologies in Fig. 5. Rainfall rates are averaged between 12°E and 42°E, and plotted as a function of latitude and time. Both the CAMS and GCM mean annual cycles are computed from monthly averages. Both series show a very similar phase and meridional range of the ITCZ, and propensity for precipitation over the southern hemisphere subtropics compared with similar latitudes in the northern hemisphere. The control integration even appears to capture the April–May maximum evident in the CAMS data, although in the model it occurs earlier and to the north. Thus, the GCM seems to simulate the oscillation between wet and dry seasons over central Africa quite well.

Figure 6 shows the corresponding time–latitude plot for the monsoon region of Asia (65°E–105°E). Here the model underestimates both the strength of the monsoon precipitation, and the northward traverse of the monsoon. There is also a tendency in the GCM for the ITCZ over the Indian Ocean to remain in the northern hemisphere throughout the year, although in individual years the ITCZ moves south of the equator (not shown). This further mutes the contrast between wet and dry seasons in this region. Spatial resolution in the model may play a role. The structure of the Tibet plateau, especially the steep southern

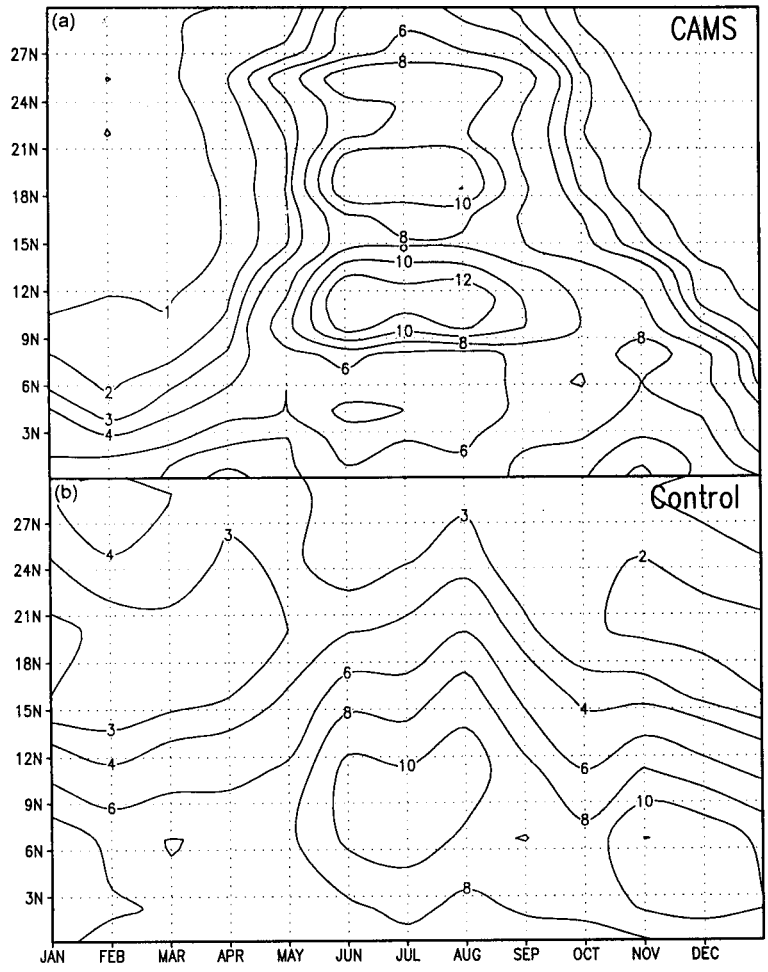

Figure 6. As Fig. 5 but averaged between 65°E and 105°E.

face, is poorly resolved at R–15, and the massif of the Indian subcontinent is practically unresolved. Nevertheless, the region between 12°N and 23°N in the control integration receives at least 60% of its annual rainfall during May–October.

4. Large-scale anomalies

In this section we focus on the climate anomalies (double-desert minus control) with particular concentration on the principal large-scale features. Anomaly patterns over specific regions will be discussed in the next section.

(*a*) *Low-latitude cooling*

The net surface albedo of the bare-soil regions is higher than the net albedo of the other vegetation types. The steppe vegetation has the second highest net albedo. Thus, the desertified areas can be expected to absorb less solar radiation than in the control case. One consequence of an increase in albedo and a decrease in absorbed radiation is a concomitant cooling of the troposphere over those areas (Charney *et al.* 1977). This is indeed the case in this experiment, although the cooling is not confined to the immediate areas of desertification. Figure 7(a) shows the anomaly of 850–200 mb thickness. The largest negative anomalies are found over south-western Asia, northern Africa and the subtropical North Atlantic. However, the region of significant (95%) negative temperature anomalies covers a large fraction of the globe, including much of the tropics and subtropics. A contiguous area extends from the central tropical Pacific across Central America and most of South America, the Caribbean Sea, the entire tropical and subtropical Atlantic, all of Africa, most of Europe, a wide zonal band of Asia from the Mideast to Korea, and a similar zonal band in the southern hemisphere from South Africa to southern Australia. This region encompasses most of the desert areas, but also covers additional territory nearly three times the area of all expanded deserts. There are only small regions of significant positive anomalies over the north-eastern US and the North Pacific. Positive surface-pressure anomalies exist over most of the desertified regions, with a broad area of small but significant negative anomalies over most of the tropics and subtropics from the Indian Ocean eastward to the eastern Pacific (not shown).

The major contribution to this cooling anomaly in the annual mean comes during the boreal summer. During this period, negative temperature anomalies in the mid-troposphere exceed 1.5 K over north-western Africa as well as Kurdistan (not shown). In addition to the significant northern hemisphere anomalies, there is also significant cooling over southern Africa and the subtropical South Atlantic. During southern summer, significant cooling anomalies are largely confined to the southern hemisphere with the exception of western Africa and the subtropical North Atlantic, where negative anomalies of 0.6 K persist in the mid troposphere.

The surface temperature decreases over most of the desertified regions, although increases do occur in some areas, particularly during summer and where cloud cover is significantly reduced (Fig. 7(b)). Meanwhile, there is an increase in net long-wave radiation upward from the surface in most of the areas, principally attributable to the decrease in downward long-wave radiation at the surface which accompanies reduced cloudiness. However, there is less total heat flux to the atmosphere because of the combination of reduced surface latent- and sensible-heat flux due to removal of vegetation. Degradation of vegetation greatly reduces transpiration, and the decrease in roughness impedes sensible heating of the planetary boundary layer. The terms of the surface energy and moisture balances averaged during the last 8 years of the integration over desertified areas globally are presented in Table 3. The net effect over the expanded deserts is a cooling of the

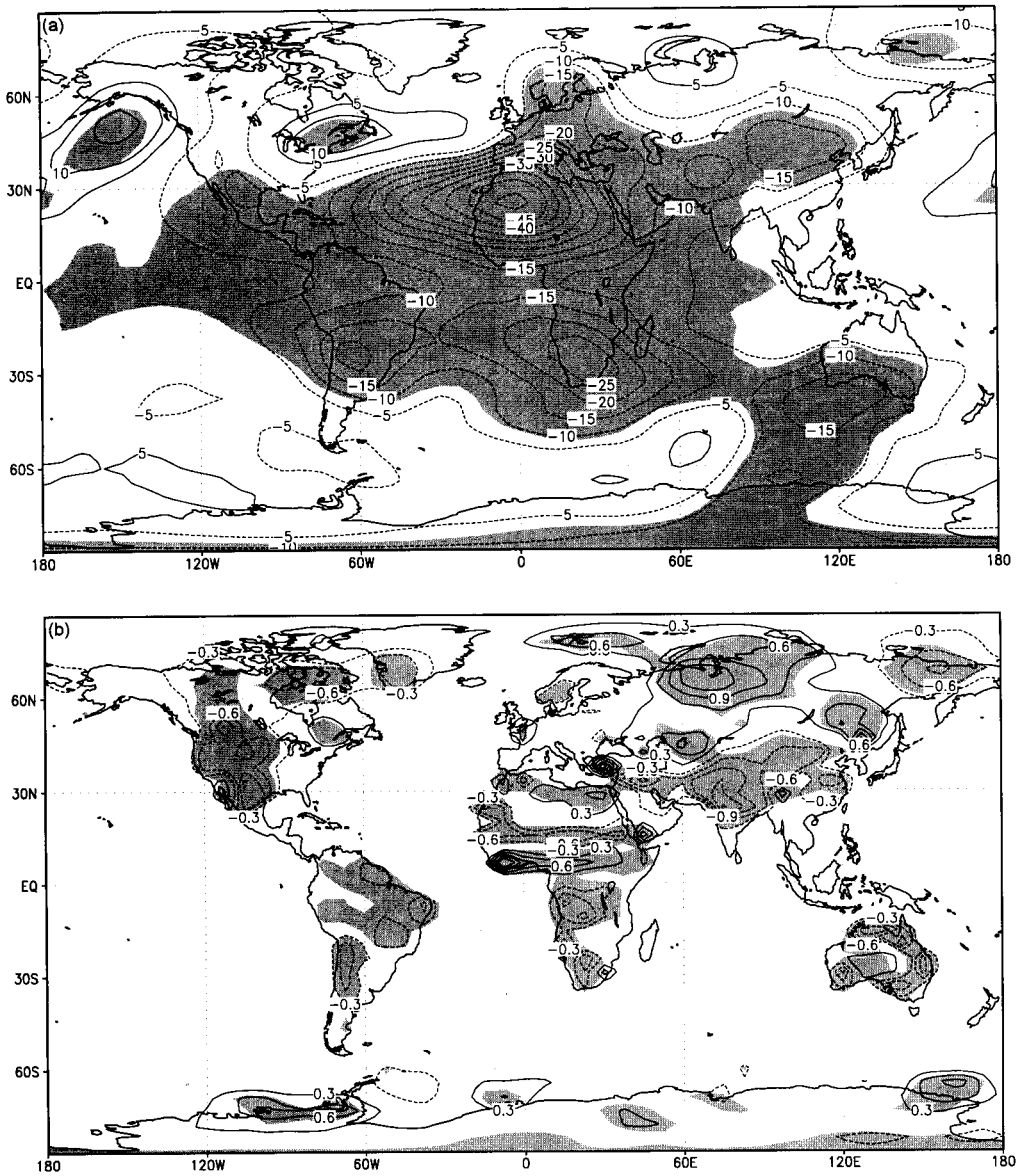

Figure 7. Mean 850–200 mb thickness anomalies (a), and surface temperature anomalies (b) for the last 8 years of integrations. Contour interval is 5 m in (a), 0.3 K in (b), zero contour is omitted. Shading indicates significance at the 95% level.

troposphere. The atmospheric circulation disperses the cooler air, spreading it westward in the tropics, and eastward in the subtropics and mid-latitude margins. The decrease in cloudiness over desertified regions, even though there is a general increase in moisture flux convergence, may be attributed to net anomalous cooling and sinking in the troposphere, along with reduced moisture flux into the atmosphere from the lower boundary.

(*b*) *Precipitation*

Anomalies for annual mean precipitation and their statistical significance are shown in Fig. 8(a). The largest contiguous negative anomalies occur over the Sahel of northern

TABLE 3. TERMS RELEVANT TO THE SURFACE MOISTURE AND ENERGY BALANCES, AVERAGED FOR ALL DESERTIFIED GRID POINTS OVER THE LAST 8 YEARS OF THE EXPERIMENTS

	Control	Desertified	Change
Precipitation	1.65 mm	1.32 mm	−20%
Evapotranspiration	1.37 mm	1.03 mm	−25%
Runoff	0.27 mm	0.30 mm	+8%
Moisture flux convergence	0.28 mm	0.29 mm	+5%
Cloud cover	41%	39%	−5%
Surface temperature	293.2 K	293.2 K	0%
Latent-heat flux	39.7 W m^{-2}	29.8 W m^{-2}	−25%
Sensible-heat flux	58.5 W m^{-2}	49.1 W m^{-2}	−16%
Short-wave down	267.3 W m^{-2}	276.0 W m^{-2}	+3%
Short-wave up	66.0 W m^{-2}	87.1 W m^{-2}	+32%
Long-wave down	325.3 W m^{-2}	318.2 W m^{-2}	−2%
Long-wave up	423.9 W m^{-2}	423.6 W m^{-2}	−0%
Net long-wave radiation	98.6 W m^{-2}	105.4 W m^{-2}	+7%

Africa. There are also significant negative anomalies over the desertified regions of southern Africa. It is interesting to note that not all desertified areas show significant decreases in precipitation. In fact, there is a region of significant increase in rainfall over south-western North America. Also, there are regions which experience significant drops in precipitation where vegetation was not altered, most notably over southern Asia. A significant shortfall exists over the northern Bay of Bengal, Myanmar, and a large part of China. Negative anomalies also appear over much of the North Atlantic.

Accompanying the regions of decreased precipitation are areas of significant positive anomalies in the annual mean. Equatorial Africa between the two deserts shows the greatest increase. This region of positive anomalies extends westward across the Atlantic, and then north-west along the coast of South America to the subtropical western North Atlantic. This north–south dipole with decrease over the desertified area, and increase to the equatorward side, is similar to that simulated by Xue and Shukla (1993) for Sahel desertification alone. There are also positive anomalies over the ocean to the west of the deserts of South Africa, Australia, and western South America. This suggests a modification of the zonal overturning circulation off the equator, perhaps driven by increased subsidence over the desertified areas. The positive anomalies extend around the oceanic poleward sides of South Africa and Australia, similar to the anomalies in the idealized subtropical desertification study of Dirmeyer (1992). Many of the other small shaded areas encompass only one or two grid points each, and are probably chance occurrence of high statistical significance.

Figure 8(b) shows the precipitation anomalies expressed as a percentage of annual mean rainfall. It shows that the greatest impact of the negative anomalies in northern Africa is to the north of the band of highest magnitude. Rainfall decreases by more than 60% over the Sudan. Almost the entire area of northern Africa and the Mideast experience at least a 20% decrease, as does much of southern Africa. Shortfalls over Australia and monsoonal Asia are generally 10%. Much of western tropical Africa experiences a 10–40% increase in rainfall. There are also 10–20% increases over the desertified region of south-western North America, and the oceanic positive-anomaly centres to the west of the southern hemisphere deserts. Table 3 shows a 20% decrease on average over all desertified areas, accompanied by a 25% decrease in evapotranspiration. There is only a small net increase in moisture flux convergence. Although it appears that reduction in evapotranspiration

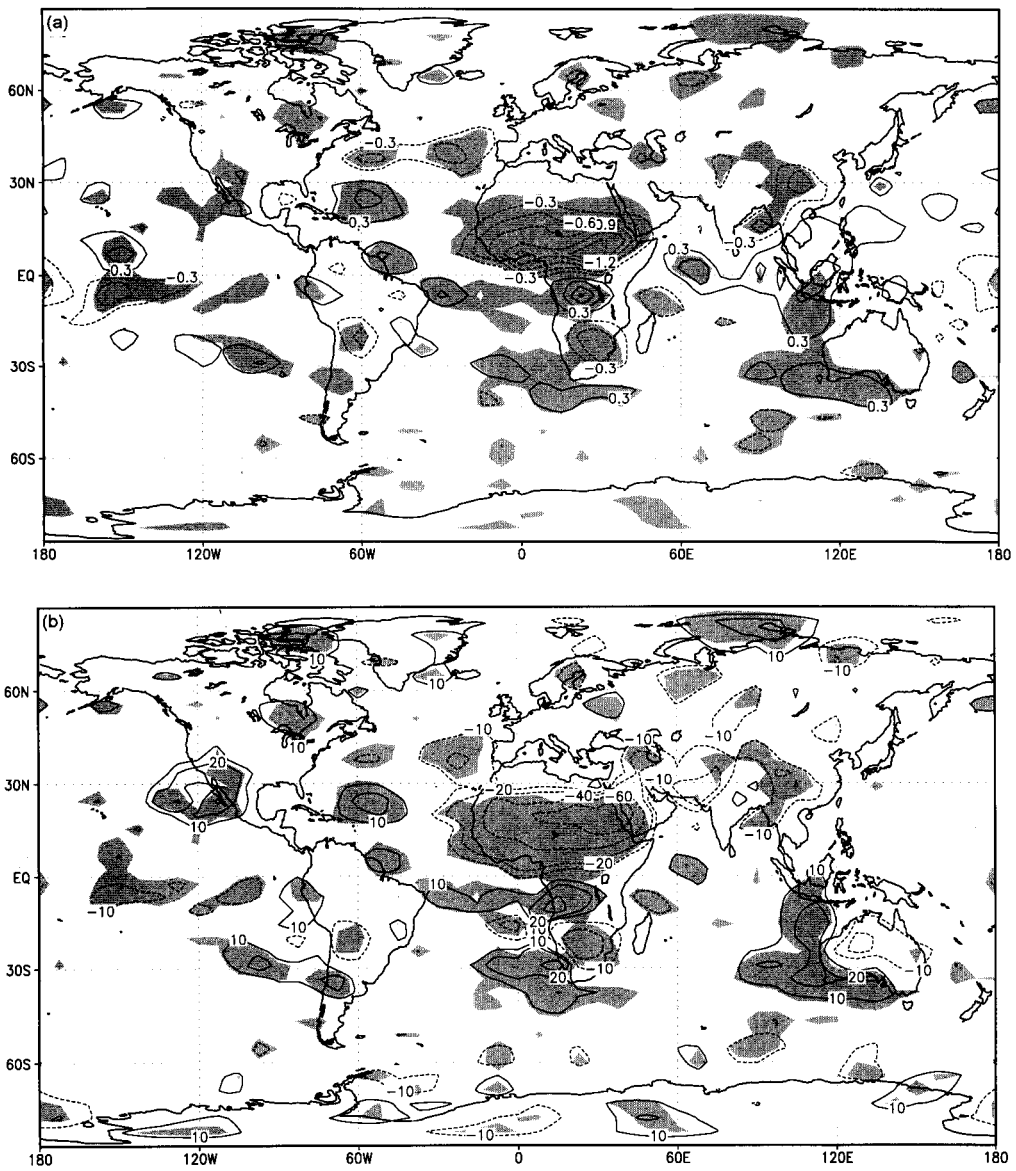

Figure 8. Mean precipitation anomalies (double-desert minus control) for the last 8 years of integrations: (a) in mm d^{-1} (contour interval is 0.3) and (b) as percentage of control rainfall (contour interval is 10%). Zero contours are omitted. Shading indicates significance the 95% level.

leads to a comparable reduction in precipitation, this is not true over all desertified areas. Over individual regions, changes in moisture flux convergence may offset or reinforce the decrease in moisture supplied by latent-heat flux. In the regions where rainfall is relatively unaffected by desertification, the decrease in available energy at the surface is primarily manifested as a decrease in sensible-heat flux. Regional differences are discussed in detail in section 5.

It should be noted that there is a reduction in the interannual variability of precipitation as well as precipitable water and most surface energy terms over northern Africa and the subtropical North Atlantic. Meanwhile, surface latent- and sensible-heat flux variability

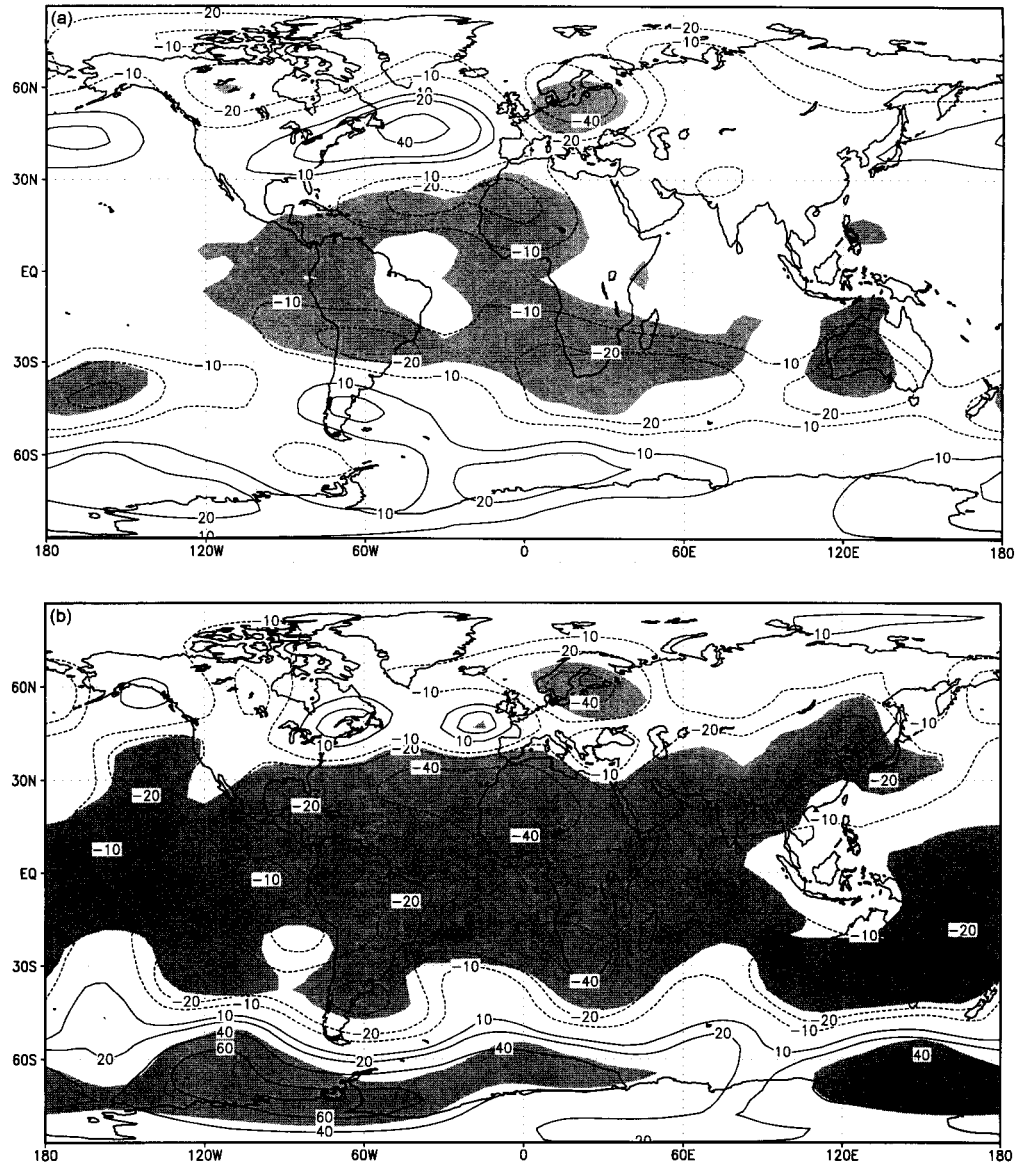

Figure 9. Mean geopotential height anomalies (double-desert minus control) at 200 mb for the last 8 years of integrations for (a) December–February and (b) June–August. Contours at ±10, ±20, ±40, ±60 m. Shading indicates significance the 95% level.

increase over equatorial Africa. Changes in variability over other parts of the globe are generally small or seasonal in nature.

(*c*) *Extratropical anomalies*

Geopotential height anomalies at 200 mb are shown in Fig. 9 for boreal winter (December, January and February (DJF)) and austral winter (June, July and August (JJA)). The broad areas of negative anomalies at low latitudes reflect the tropospheric cooling described previously. There are also significant anomalies in the extratropics, particularly during austral winter. However, we will first focus on DJF (Fig. 9(a)). There

is a significant negative height anomaly centred over the Baltic region. The maximum anomaly is 52 m, and much of Europe is covered by a significant decrease in geopotential height. This area is associated with a negative tropospheric temperature anomaly, and an increase in interannual variability over western Russia during the same season (not shown). There is an equally strong positive height anomaly over the North Atlantic, but only a very small area south of Nova Scotia is statistically significant. A weak negative anomaly also exists over north-western Canada. In the summer hemisphere, a negative anomaly comparable with the one over the Baltic Sea exists to the east of New Zealand.

During JJA (Fig. 9(b)), the high latitudes of the southern hemisphere are covered by positive height anomalies, with significant deviations along much of the Antarctic coast and adjacent oceans. The Antarctic anomalies appear to be part of a meridional redistribution of mass to compensate for the falling surface pressures in the tropics. Anomalies in surface pressure (not shown) show significant increases over the southern oceans during JJA, with smaller increases in other seasons. It is interesting to note that height anomalies similar to DJF exist over the high latitudes of the northern hemisphere. Although the magnitude of these summer anomalies is less than their winter counterparts, the regions of statistical significance cover about the same area. In fact there is a significant decrease in the interannual variability of surface pressure over the North Atlantic. The anomalous ridge over the North Atlantic and troughs over Canada and northern Europe also exist in the equinoctial seasons, although the European trough is rather weak during spring. The robust nature of these features suggest they may be part of an anomalous stationary-wave pattern forced from the large desertified region in northern Africa. Northern Africa is the likely origin owing to its proximity and the dominant strength of the heating anomalies there. In fact, anomalies in 200 mb northern hemisphere vorticity (not shown) are strongest at all latitudes in the sector between 60°W and 60°E on both seasonal and annual time-scales.

Overall, the meridional temperature gradient decreases, especially in winter. There is a cooling in the tropics, subtropics, and summer extratropics, with warming over the winter extratropics. The tropospheric jet stream shifts northward in both hemispheres. Specifically, the jet and storm track shift equatorward over the Indian Ocean during austral summer, and in the vicinity of Australia during all seasons. The jet shifts north over the North Atlantic during winter and summer, and over the North Pacific during boreal winter only. There is a slight decrease in the strength of the jet in each hemisphere during winter, consistent with the reduced temperature gradient. Atmospheric humidity generally decreases over the desertified areas, and increases in the tropics, particularly over the convective centres of tropical Africa, the Amazon basin and Indonesia.

5. Regional anomalies

(*a*) *Africa*

The semi-arid regions of both northern and southern Africa where desert was expanded are regions of strong seasonality in rainfall. These regions experience a distinct rainy season during summer, and a dry season during winter (Nicholson 1986). These seasons are a manifestation of the differential heating of land between the two hemispheres, and the migration of the ITCZ north and south over land. Western Africa differs somewhat in that there is a meridional land–sea contrast rather than a warm land–cool land contrast, but the coastal region is close enough to the equator that the ITCZ migrates over land in that area as well (Meehl 1992).

Figure 10 shows the mean annual cycle of the surface moisture balances for the control case and the anomaly (double-desert minus control) for the desertified regions of northern and southern Africa. The annual cycle is averaged over only those areas where vegetation

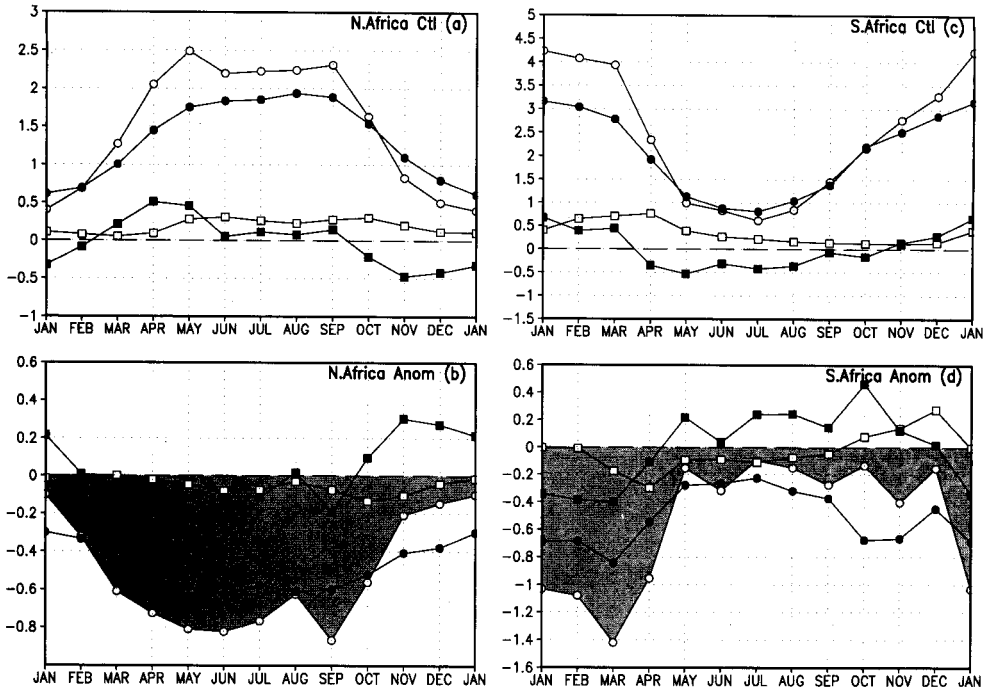

Figure 10. Time series of mean monthly surface-moisture-balance terms for: (a) northern Africa control case, (b) northern Africa anomaly (double-desert minus control), (c) southern Africa control case and (d) southern Africa anomaly. Units are mm d^{-1}. Open circles: precipitation; filled circles: evapotranspiration; open squares: runoff; filled squares: change in soil moisture. Negative precipitation anomalies are shaded.

has been changed between experiments. The area for northern Africa includes desertified points within the box 20°W–49°E, 0°N–50°N (see Fig. 1). The desertified regions of western Asia which are outside the Asian monsoon regime are included with northern Africa. Areas of Africa south of the equator are averaged in Figs. 10(c) and (d). There are clear wet and dry seasons in each region (Figs. 10(a) and (c)), with variations in mean monthly rainfall of nearly an order of magnitude in both north and south. The rainy and dry periods are synonymous with periods of high and low evapotranspiration respectively. Soil moisture is seen to recharge during the onset of the wet season, and deplete during the dry season. Runoff is highest after the initiation of the wet season. Precipitable water over northern Africa (not shown) is reduced by 10–15% throughout the year, with the largest anomalies during summer. Over southern Africa, precipitable water is reduced 5–15% with the greatest reduction in March.

Desertification in Africa is found to cause negative anomalies in precipitation during both wet and dry seasons (Figs. 10(b) and (d)). Although the magnitudes of the anomalies are much smaller during the dry season, the percentage decrease in rainfall is not a strong function of season. In the north, the minimum reduction in monthly rainfall is 25% in November, with the largest decrease being nearly 50% in March. Reductions in the south vary between 5 and 40%. The mean values of precipitation and evapotranspiration vary in a similar fashion throughout the year, since this is a moisture-limited regime where evaporation can only occur when precipitation has occurred. Yet, the evapotranspiration anomaly has a much smaller annual swing than the precipitation anomaly. The same is true of runoff and change in soil moisture. The effect of the consistent decrease in evapotranspiration is to decrease the annual variation of precipitation minus evaporation

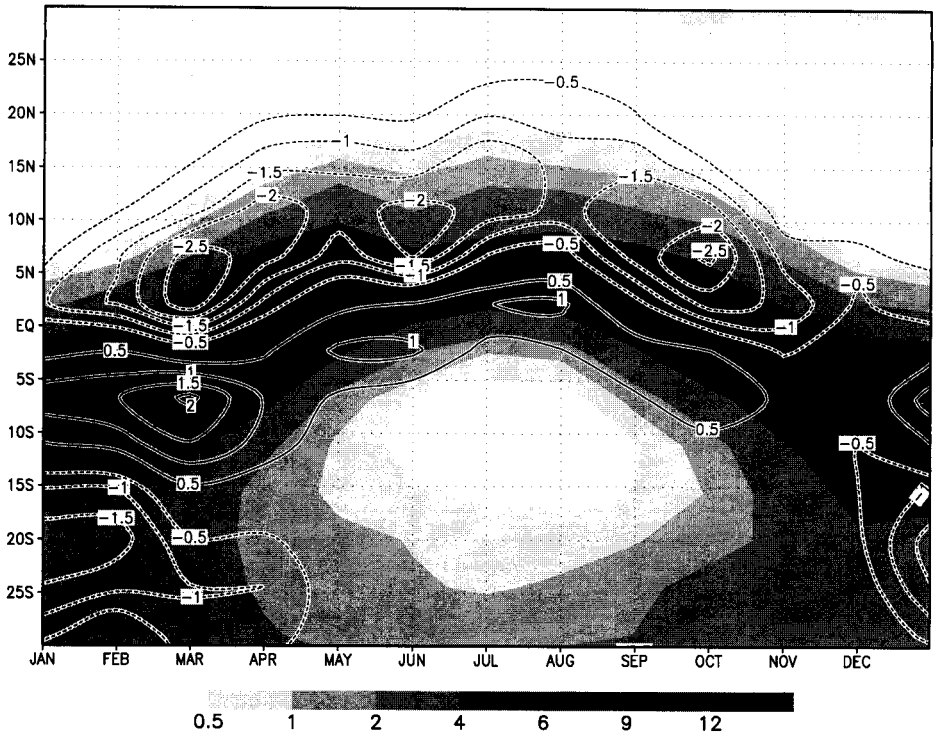

Figure 11. Mean annual cycle of double-desert precipitation (shaded) and anomaly (contours) as functions of latitude averaged between 12°E and 42°E. Units are mm d^{-1}.

$(P - E)$. Thus, atmospheric moisture-flux convergence decreases during the rainy season, and the export of moisture through flux divergence during the dry season is reduced. This means that, over Africa, there is a reduction in the amount of cross-equatorial moisture advection from the winter to the summer hemisphere. The ITCZ rainband does not suffer, however. As shown in Fig. 8, rainfall in the African ITCZ increases. Figure 11 shows the annual cycle of precipitation over Africa averaged between 12°E and 42°E in the double-desert case, and the anomaly. There is a narrowing of the range of the ITCZ, accompanied by intensification and a slight shift southward. Rainfall decreases on the poleward margins of the ITCZ in the summer hemisphere. This occurs despite the fact that surface temperatures in the summer hemisphere subtropics are 1–2 K warmer, and winter surface temperatures 1–2 K cooler in the double-desert case, which might be expected to drive a stronger seasonal circulation. The increase in seasonality of surface temperatures is a typical characteristic of arid regions with limited soil moisture. The equatorward margin of the desertified region of northern Africa maintains positive anomalies of 0.5–1 K in winter and summer.

Figure 12 shows the annual cycle of terms in the surface energy balance for the control case and anomalies over northern and southern Africa, defined as in Fig. 10. The solar driving force of the differential heating is evident in the cycle of absorbed short-wave radiation. Weaker cycles of sensible- and latent-heat flux are evident in the control cases (Figs. 12(a) and (c)). The increase of albedo in the desertified areas leads to negative anomalies in absorbed short-wave radiation (Figs. 12(b) and (d)). The decrease is accompanied by a reduction in sensible-heat flux in both areas. The reduction in evapotranspiration seen in Fig. 10 is represented by the negative anomaly in latent-heat flux. The magnitude

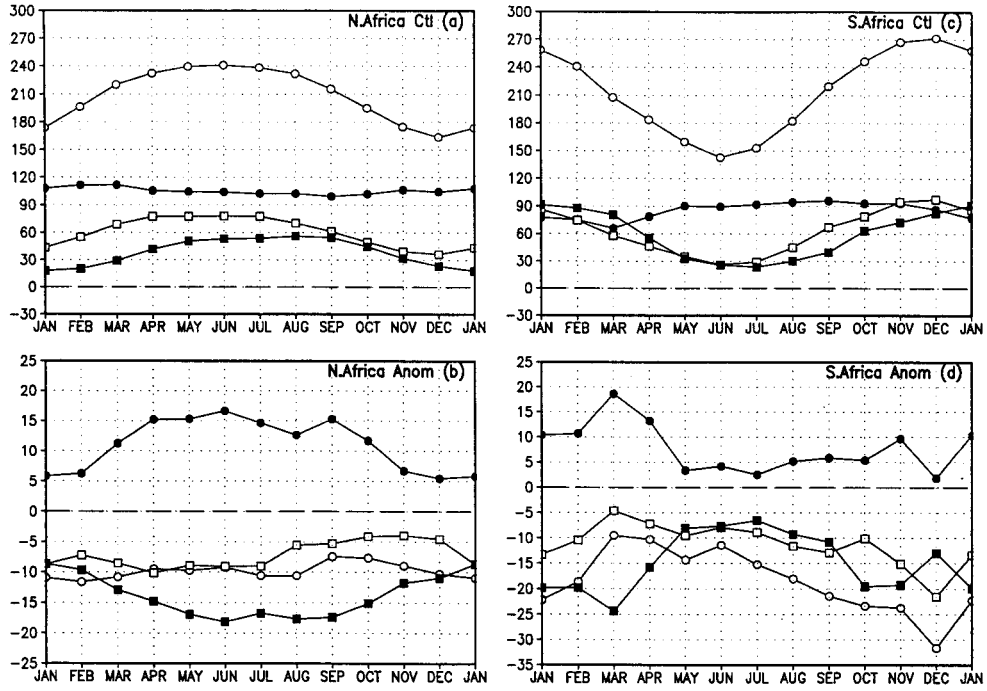

Figure 12. Time series of mean monthly surface-energy-balance terms for: (a) northern Africa control case, (b) northern Africa anomaly (double-desert minus control), (c) southern Africa control case and (d) southern Africa anomaly. Units are W m^{-2}. Open circles: absorbed short-wave radiation; filled circles: net long-wave radiation (upward); open squares: sensible-heat flux; and filled squares: latent-heat flux.

of the negative latent-heat-flux anomaly matches the anomalies in sensible-heat flux and absorbed short-wave radiation during the dry season, and exceeds them during the wet season. Surface temperature increases because the reductions in surface fluxes outpace the reduction in absorbed solar radiation, which is tempered by decreased cloudiness and increased short-wave radiation reaching the ground, particularly in summer. As a result, there is an increase in net long-wave radiation escaping the surface. Also, the anomalies in latent-heat flux and net long-wave radiation reduce the magnitude of the annual cycle in these terms.

The differences in the energy balances between the Sahel and Sahara regions are not shown by Fig. 12. These areas have surface temperature anomalies of the opposite sign (see Fig. 7(b)). The Sahel warms, whereas the Sahara cools like most other desertified regions. Table 4 shows the annual means of key terms for the Sahel (defined as the grid points over Africa between 4° and 13°N where mean surface temperature increased) and the Sahara (grid points between 9° and 27°N where mean surface temperature decreased).

Over the Sahel, mean cloud cover drops by 14%, resulting in a similar percentage increase of downward short-wave radiation at the ground. Recall that surface albedo has been increased as a result of desertification, so that the amount of short-wave radiation absorbed at the surface drops by 8.4 W m^{-2}. The reduction in cloudiness also reduces downward long-wave radiation at the surface by 14.9 W m^{-2}. At the same time, the sum of latent- and sensible-heat flux away from the surface drops by 28.6 W m^{-2}. Virtually all of this decrease is due to reduced evapotranspiration—soil moisture availability is greatly reduced. Thus, there is a surplus of about 5 W m^{-2} of energy at the surface; this leads to the small net warming and is then thermally radiated away.

TABLE 4. ANNUAL AVERAGES FOR THE CONTROL EXPERIMENT, AND CHANGE DUE TO DESERTIFICATION OVER NORTHERN AFRICA (SEE TEXT FOR DEFINITIONS OF AREAS)

	Sahel		Sahara	
	Control	Change	Control	Change
Short wave incident at surface (W m^{-2})	253.1	+26.8 (−11%)	295.4	+17.3 (−6%)
Short wave absorbed by surface (W m^{-2})	203.9	−8.4	229.8	−12.6
Latent+sensible-heat flux from surface (W m^{-2})	135.4	−28.6	130.6	−29.6
Downward long wave at surface (W m^{-2})	382.7	−14.9	345.8	−19.0
Soil wetness	0.65	−0.23	0.37	−0.13
Cloud-cover fraction	0.61	−0.09 (−14%)	0.36	−0.6 (−18%)

Further north over the southern and central Sahara, absorbed short-wave radiation drops by 12.6 W m^{-2}, while the sum of latent- plus sensible-heat flux drops by 29.6 W m^{-2}. In fact, latent heating drops by only two thirds the amount in the Sahel, as the soil is already quite dry in the control case, but reduced sensible-heat flux makes up the difference. Nonetheless, this balance is not greatly different from that of the Sahel. The difference between the two regions is suggested by the relative changes in cloud cover and incident short-wave radiation at the surface. Over the Sahara, cloudiness drops by 18% but sunlight at the surface drops by only 6%. This discrepancy is present during all seasons, and implies that cloud cover decreases principally at night. The effect is to promote long-wave cooling of the surface during the night. The decrease in mean cloudiness during the day is much more modest, so there is not a large increase in absorbed short-wave radiation to warm the surface and offset the cooler nights. The net result is cooling of the surface. In the other desert regions of the world, the magnitudes of the decreases in absorbed short-wave radiation and surface heat fluxes are comparable, and the decrease in downward long-wave radiation is large enough to compensate for any differences and promote surface cooling.

(*b*) *Asia and Australia*

Both southern Asia and Australia are situated such that they lie predominantly in the subtropics adjacent to equatorial oceans. These areas experience well defined monsoons, driven by the seasonal oscillation of contrasts between the heating of land and sea. Thus, the annual cycle over these regions differs from that of the land–land cycle over Africa. The monsoons of southern Asia are intensified by the elevated heat source of the Tibetan plateau to the north (Murakami 1987; Yanai and Li 1994). The Australian monsoon may be somewhat weakened by the presence of the many islands of Indonesia, which act as numerous small heat sources for the atmosphere and help anchor the centre of low-level convergence near the equator (Meehl 1992). Nonetheless, in determining the response of climate to desertification, the differences between Australia and Asia appear to be less important than their shared differences from Africa.

Figure 13 shows the surface moisture balances for southern Asia and Australia. Again, only land points where vegetation has been changed are included in the calculation, over 60°E–120°E, 5°N-40°N for Asia, and 100°E–160°E, 10°S–40°S for Australia (see Fig. 1). Both areas show strong seasonality with precipitation and evapotranspiration in phase, like Africa. Australia shows little variation in soil moisture or runoff. Both regions are also similar to Africa in having large negative rainfall anomalies during summer. However, neither Asia nor Australia have appreciable negative anomalies during the dry season. In fact, both regions show small to moderate positive rainfall anomalies in some months.

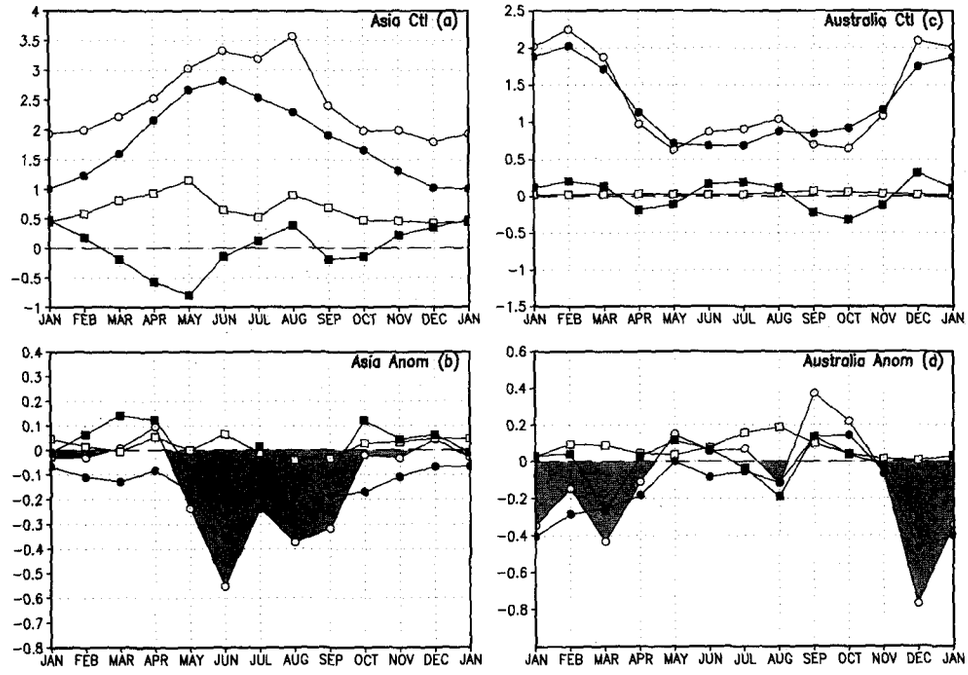

Figure 13. Time series of mean monthly surface-moisture-balance terms for: (a) Asia control case, (b) Asia anomaly (double-desert minus control), (c) Australia control case and (d) Australia anomaly. Units are mm d^{-1}. Open circles: precipitation; filled circles: evapotranspiration; open squares: runoff; filled squares: change in soil moisture. Negative precipitation anomalies are shaded.

Another critical difference is the relatively small and seasonal evapotranspiration anomalies over Asia/Australia compared with Africa. Although negative anomalies exist over Asia in all months, they do not exceed 10% in any month. This is in contrast to the 25–50% shortfalls over Africa. In Australia, evapotranspiration anomalies are negligible throughout the dry season, and are actually positive during September and October. Negative anomalies do approach 25% at the onset of the wet season but are otherwise small. One might assume that since these are areas where deserts have been intensified more than they have been expanded, that evapotranspiration was already limited in the control case, and there is little room for change. However, control-case evapotranspiration rates over Africa (particularly northern Africa) are as low or lower than over Asia and Australia, yet Africa experiences a sharp decrease in evapotranspiration. We do not believe vegetation contrasts are the sole factor in determining the differing responses; land–sea geometry and orography also play a role.

Figure 14 shows the annual cycle of rainfall in the double-desert case averaged over monsoonal Asia (65°E–105°E), as well as the anomalies. There is a decrease in rainfall along the entire leading edge of the monsoon. Rainfall in the south is reduced during April and May. The deficit migrates north during the peak of the monsoon, while rainfall over extreme southern India, Sri Lanka, Malaysia and the Indian Ocean increases. Deficits spread south again with the receding monsoon during fall.

The surface energy balance over Asia and Australia is presented in Fig. 15. The change in surface latent-heat flux over Asia is small compared with what was seen for Africa. Somewhat larger anomalies are seen for Australia, but changes in latent-heat flux are still smaller than the changes in sensible-heat flux in all months. As over Africa,

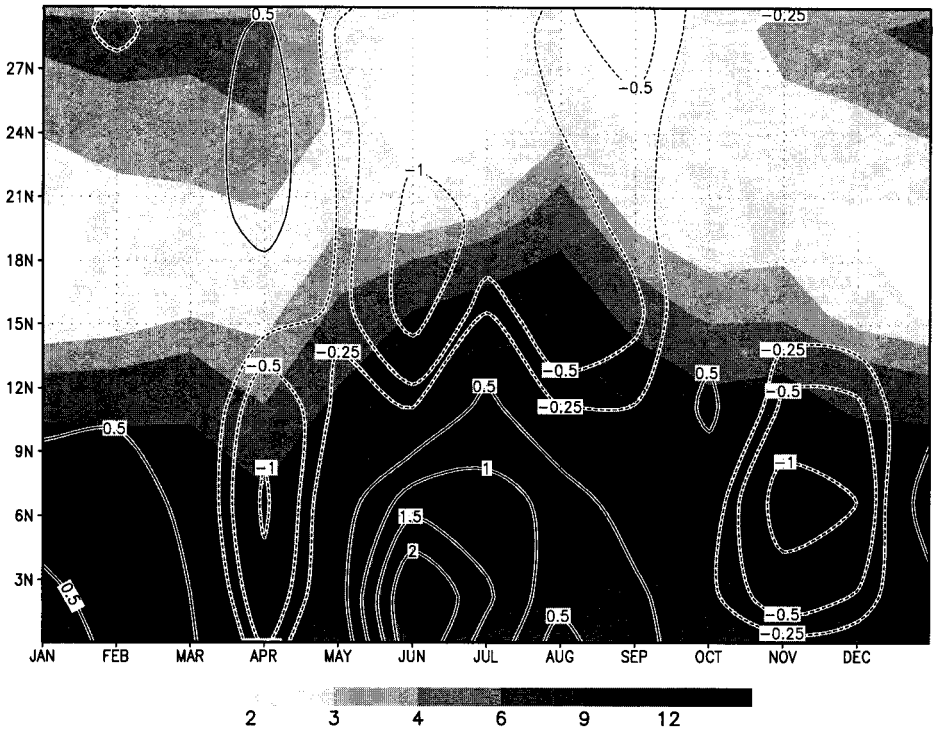

Figure 14. Mean annual cycle of double-desert precipitation (shaded) and anomaly (contours) as functions of latitude averaged between 65°E and 105°E. Units are mm d^{-1}.

decreases in absorbed short-wave radiation are matched closely by reductions in sensible-heat flux. But there is relatively little change in latent-heat flux, especially during the dry season, so net long-wave radiation is not affected. An exception is during the wet season over Australia, where the increase in long-wave flux resembles the patterns in Africa. Australia has a more complicated pattern of surface temperature anomalies than Africa (not shown). There is generally an increase in surface temperature over central Australia, with cooling along the coasts. This pattern is present to some degree in all seasons. Most of monsoonal Asia is slightly warmer during summer and cooler during winter, except for south-western Asia for which the opposite pattern occurs.

(*c*) *The Americas*

The desertified regions of the Americas have a different geometry than those of the eastern hemisphere. Whereas the deserts of Africa, Asia and Australia lie predominantly in zonal bands, the mountain ranges of the Andes and Rockies constrain the zonal extent of the American deserts. Also, there is little land in the subtropics. The continents are narrow at Mexico and the Pampas: they are wide in the tropics at the Amazon basin and in the mid latitudes of the United States and Canada. Consequently, there are no comparably balanced areas of land in the subtropics and tropics as in Africa, nor are there clear meridional delineations between subtropical land and tropical ocean as with Asia and Australia. This geometry limits both the area of strong seasonality of precipitation, and the intensity of the seasonality. The margins of the Amazon basin exhibit wet–dry oscillations similar to Africa (Nobre *et al.* 1991), but the Andes divide the eastern subtropical lands, characterized by strong maritime influence and dependable rain, from the severe deserts of the west coast.

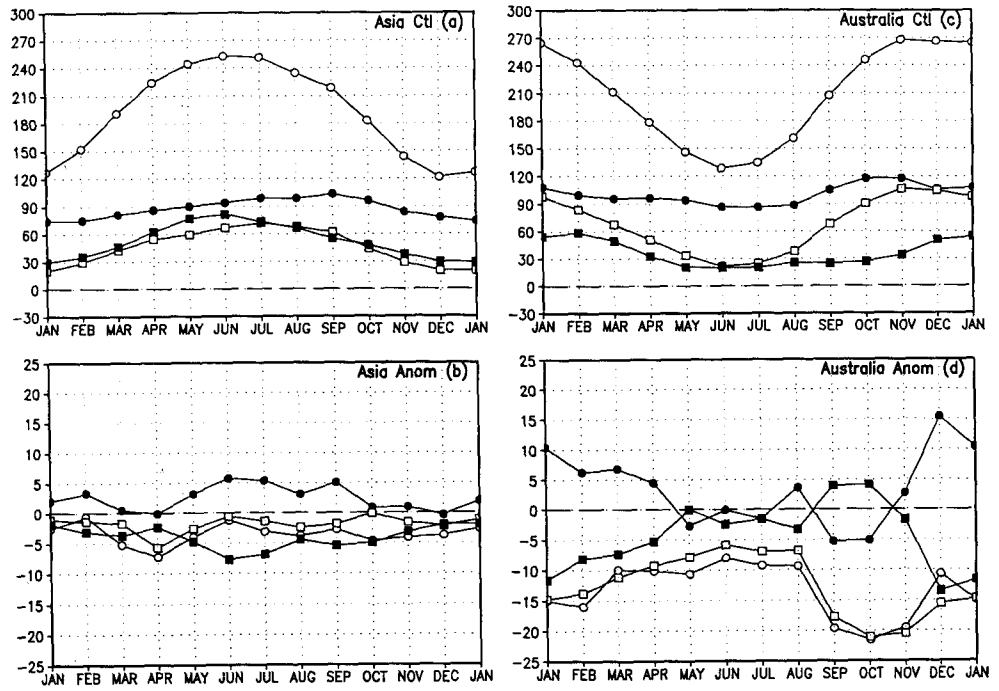

Figure 15. Time series of mean monthly surface-energy-balance terms for: (a) Asia control case, (b) Asia anomaly (double-desert minus control), (c) Australia control case and (d) Australia anomaly. Units are W m^{-2}. Open circles: absorbed short-wave radiation; filled circles: net long-wave radiation (upward); open squares: sensible-heat flux; and filled squares: latent-heat flux.

The Nordeste region of Brazil is a semi-arid tropical region with a unique climate strongly dependent on conditions in the tropical Atlantic (Moura and Shukla 1981; Hastenrath and Greischar 1993). Extreme south-western North America has a weak summer-monsoon circulation (Bryson and Lowery 1955; Douglas *et al.* 1993), but nothing as dramatic and dependable as in Asia or northern Australia.

The desert regions of south-western North America, western South America, and the Nordeste region of Brazil have been examined separately. Desertified points as indicated in Fig. 1 are included for each region. Figure 16 shows the annual cycle of the moisture balance in these three areas. There is not a dominant summer rainy season in the model for any of these areas. Also, none of these areas exhibit the strong phase-locking of evapotranspiration to precipitation that was evident in the other regions, as there is no appreciable decrease in soil moisture. The Nordeste shows a weak tendency for phase-locking, but evapotranspiration does not reflect the heavy precipitation of March–May.

We find that in the doubled-desert case, there is little drought signal in the Americas. The anomaly plots (Figs. 16(b), (d) and (f)) show sporadic precipitation anomalies in each area. The desert region of North America has positive rainfall anomalies in most months, with increased runoff but little change in evapotranspiration. Western South America shows a persistent negative anomaly during the summer and positive anomalies during winter, similar to that of Asia and Australia, but the annual cycle of the precipitation anomaly is out of phase with the evapotranspiration anomaly. The summer drought appears to be confined to the Altiplano of Bolivia, which is geographically similar to South Africa in that there is a large tropical land region to the north. However, the annual cycle of anomalies in precipitation resemble the land–sea monsoon region.

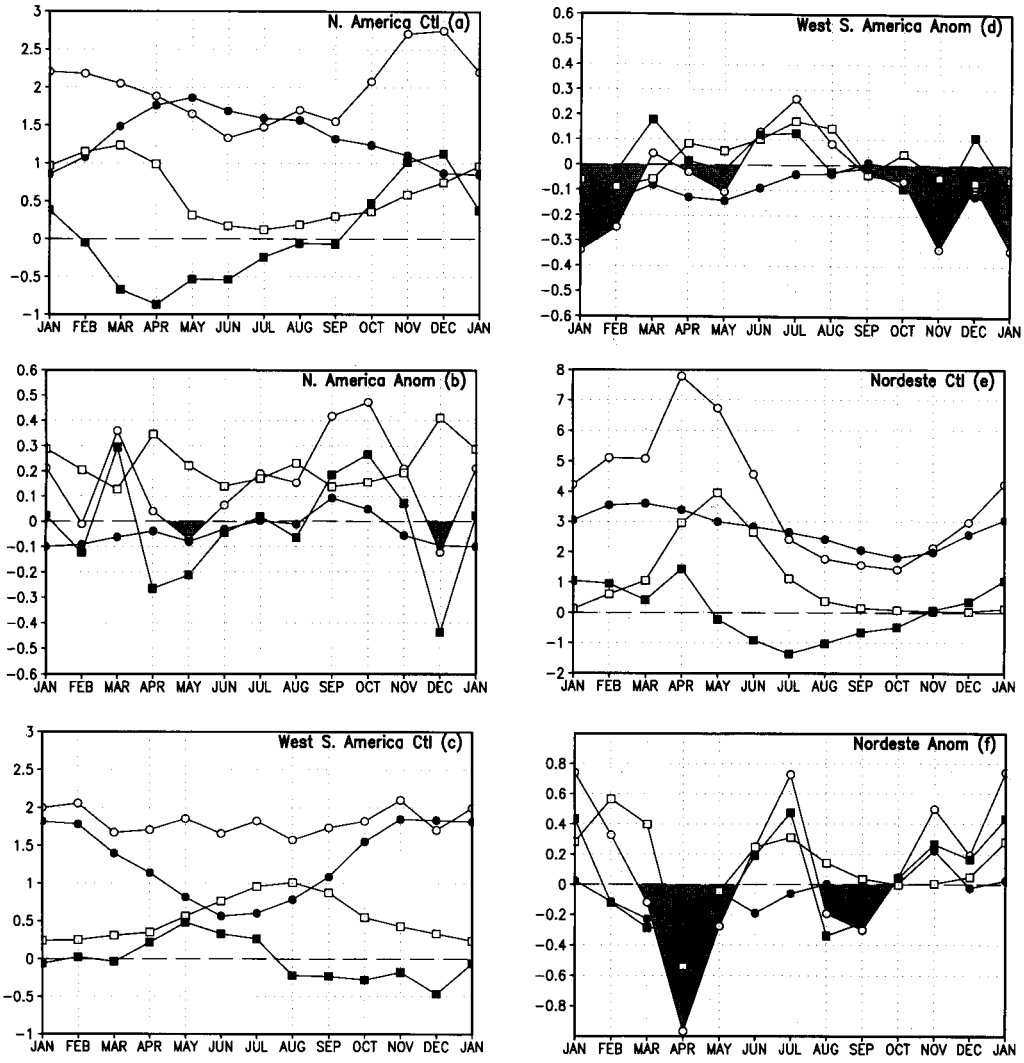

Figure 16. Time series of mean monthly surface-moisture-balance terms for: (a) North America control case, (b) North America anomaly (double-desert minus control), (c) western South America control case, (d) western South America anomaly, (e) western Nordeste control case and (f) Nordeste anomaly. Units are mm d^{-1}. Open circles: precipitation; filled circles: evapotranspiration; open squares: runoff; filled squares: change in soil moisture. Negative precipitation anomalies are shaded.

Large monthly anomalies exist over the Nordeste, but there is little pattern. If anything, there seems to be a semi-annual signal, with negative anomalies in the wet and dry seasons, and positive anomalies during the transitions. Recall (from Fig. 8) that while there is a weak negative rainfall anomaly over the region, there are significant positive anomalies just off the coast. These centres, which are fairly robust across seasons, may be contributing to the intermittent positive anomalies. Much longer integrations would be necessary to establish significance in these weak patterns.

The three regions of desertification in the Americas have the smallest anomalies of evapotranspiration. In these regions, most of the deficit in absorbed radiational energy at the surface is consumed by a decrease in sensible-heat flux. Undoubtedly, the feedback loop between precipitation and evapotranspiration accounts in large part for the large

anomalies in these fields in the other regions, as well as the small anomalies over the Americas. However, the desertified regions of North America and the Nordeste also have the largest positive anomalies in moisture-flux convergence, again showing the significance of factors other than evapotranspiration in contributing to the wide range of responses to desertification.

6. Mechanisms

The grouping of precipitation anomalies with respect to regional climate regimes suggest there are three categories of response to desertification. First, there are the regions which experience year-round negative anomalies in precipitation. Both northern and southern Africa fit into this category. Second, there are regions which experience significant decreases in precipitation only during the summer. The 'classical' land–ocean monsoon areas of southern Asia and Australia, along with western South America, are in this category (by classical we mean monsoon circulations driven by land–sea contrast, and not the migration of a land-locked ITCZ between hemispheres as occurs in the monsoons of Africa). Last, there are the areas exhibiting little or no systematic shortfalls of precipitation during any season. These include the desertified regions of North America and the Nordeste, which have weak monsoon circulations.

We speculate that the variation in the response of climate to desertification is directly attributable to the differences in the regional atmospheric circulations brought about by the different land–sea distributions. It is well established (Young 1987) that in a monsoon circulation, whether it be land–sea or land–land, there is rising air over land in the tropics and subtropical margins of the summer hemisphere. This lifting is forced by the strong solar heating of this land relative to land in the winter hemisphere, and the more thermally stable oceans. This warming of the surface helps pump heat into the atmosphere, both directly by contact, and latently through increased evaporation and transpiration. The rising air is the seat of convection and precipitation in the monsoon. To balance this rising air there must be subsidence elsewhere. This occurs further over the subtropics, particularly in the winter hemisphere, establishing the classic Hadley circulation. In this overturning circulation a great deal of low-level moisture is drawn across the equator to the summer hemisphere from evaporative source regions in the winter hemisphere. This moisture supplies the monsoon precipitation.

We suggest the following mechanism to account for the differing regional responses. Desertification in the subtropics reduces both the sensible-heat transfer to the atmosphere, and the rate of evapotranspiration, reducing the forcing of rising motion in two ways. This has the effect of increasing subtropical subsidence where it already exists, and reducing any lifting that may otherwise occur near the tropical–subtropical boundary. The region of lifting and precipitation retreats into the tropics, and intensifies to maintain the balance between rising and descending air. The increased convection in the tropics serves to intercept some of the cross-equatorial supply of moisture in the monsoon circulation. Coupled with decreased local evaporation, the atmosphere in the summer hemisphere subtropics is starved for moisture, and precipitation decreases.

The mechanism described above applies to various degrees in the different regions. Over much of subtropical Africa, land lies on both sides of the equator, so the desertification of northern and southern Africa each reduce evaporation, affecting both local cross-equatorial moisture sources. Thus, the intensified tropical convection exists during every season, and these regions suffer an atmospheric moisture deficit year-round. Precipitation over subtropical Africa in both hemispheres suffers accordingly. Over the 'classical monsoon' regions of southern Asia and Australia, the effect during local summer is much

the same as seen in Africa. Reduced heat flux from the desertified lands biases them toward atmospheric subsidence and reduced rainfall. There is an increase in rainfall near the equator, which for these regions is an oceanic zone that has abundant rainfall throughout the year, and is evident in the annual mean in Fig. 8(a). During winter, however, there is no corresponding desert at the same longitude in the opposite hemisphere for either southern Asia or Australia. Thus, there is no catalyst to enhance convection in the tropics and drain away local atmospheric moisture. Winter precipitation is unaffected. It should be noted that both Asia and Australia tend to come under the influence of mid-latitude storm systems during winter, whereas subtropical Africa generally does not. This gives the climates of Asia and Australia more independence than Africa from local surface conditions during winter.

As stated earlier, the desertified regions of the western hemisphere are small, and not longitudinally broad like the semi-arid regions of the eastern hemisphere. Also, the coastlines in the subtropics are oriented predominantly north–south rather than east–west. Thus, there is not a well-established monsoon circulation in the western hemisphere driven by annually varying heating over large subtropical land masses. This makes the climates of North and South America relatively insensitive to desertification in this experiment. The exception seems to be the Altiplano of Bolivia, which has extensive tropical lands adjacent to it like the subtropical African regions. However, there is no corresponding subtropical land in the northern hemisphere—instead there is the Caribbean Sea. Thus, the region takes on the character of the land–sea monsoon regions and suffers only a seasonal drought due to desertification. There is an increase in rainfall over the tropical Amazon basin during the season of negative precipitation anomalies over the Altiplano, consistent with increases in tropical rainfall, discussed earlier, in the eastern hemisphere, but this increase is not well reflected in the annual mean rainfall anomalies shown in Fig. 8.

Decreased surface heating over the intensified deserts of the subtropics may also lead to increased local subsidence by another means. The presence of cooler mid-troposphere air over adjacent oceans and land unaffected by desertification, described previously, decreases the static stability of the atmosphere in those areas. Meanwhile, moist static energy decreases over the desertified regions. The contrast in moist static energy between the deserts and surrounding areas is enhanced, making the surrounding areas even more favourable for moist convection. Such a rise in convection over adjacent areas can reinforce the overturning circulation and, by continuity, augment subsidence over the desert regions, further depriving them of moisture and rainfall. We have not thoroughly investigated the potential strength of this second mechanism, but offer it here as conjecture.

7. Summary

In this study we have examined the effect on climate of doubling the extent of the world's deserts by use of a GCM with a realistic representation of fluxes between the atmosphere and land surface/biosphere (SSiB). The double-desert case represents an extreme scenario of desertification which might ensue as a result of combined natural and anthropogenic causes. Desert-type vegetation is intensified and expanded in five regions: northern and southern Africa, southern Asia, Australia and south-western North America. Desert is also introduced in western South America (where its current extent is too zonally small to be resolved by the GCM), and the Nordeste region of Brazil.

We have found that the doubling of desert area results in significant cooling over much of the tropics and subtropics. The anomalously cool air is not limited to only the desert regions, but is dispersed by the atmospheric circulation to cover an area nearly six times the size of the current deserts as represented by the SSiB. This cooling weakens

slightly the temperature contrast between the equator and the poles in the troposphere. Global mean air temperature drops 0.2 K at 700 mb and negative anomalies of at least 0.1 K occur from 900 to 250 mb.

Another effect of expanding deserts is a change in the distribution of precipitation. Rainfall generally, but not invariably, decreases over desertified areas. Over Africa the decreases are large. Moderate decreases occur over south-east Asia and Australia. Precipitation increases over south-western North America. There are also increases over equatorial Africa, the tropical Atlantic and Indian oceans, and over ocean to the west and south-west of the desertified areas of the southern hemisphere.

There are significant anomalies in the extratropical circulation as well. Tropospheric temperatures over Europe are cooler, and an anomalous trough persists over northern Europe throughout the year. A ridge of large comparable magnitude but marginal significance is situated over the North Atlantic. There are significant positive height anomalies over the high latitudes of the southern hemisphere during southern winter.

Areas of desertification experience an increase in net surface albedo, and decreased surface roughness. These changes combine to reduce the flux of energy from the surface by decreasing the percentage of solar radiation absorbed, and limiting the mechanical transport of thermal energy away from the surface by sensible heating. Transpiration is also reduced by the removal of vegetation, so latent-heat flux is also curtailed. The reduction in heat flux from the surface leads to a cooling of the overlying atmosphere. Depending on the relative strengths of the reductions in absorbed solar radiation and heat flux, the surface temperature may rise or fall. Both situations occur in the double-desert case. Some areas are consistently warmer or cooler, while others experience an increase in the annual cycle of surface temperature: warmer in summer and cooler in winter. Regardless, cloud cover generally decreases, allowing more long-wave radiation from the surface to escape into space, further cooling the troposphere.

Africa appears to suffer the greatest impact in this study. Precipitation is reduced by more than 50% over much of the Sahel. In both northern and southern Africa, the negative precipitation anomalies are a year-round feature. The magnitudes of the anomalies vary in accordance with the rainy and dry seasons, but the percentage reductions in rainfall are rather stable throughout the year. Between the dry, desertified areas is a region of increased rainfall over tropical Africa where the surface was not changed. The ITCZ appears to narrow and intensify, while crossing a smaller meridional range with the seasons. The intensified low-level convergence over equatorial Africa appears to be directly connected to increased subtropical subsidence in both hemispheres.

Asia and Australia, like Africa, experience pronounced drought during the summer rainy season. The mechanism is similar, although it appears to be the reduced contrast in heating between desert land and ocean, rather than desert land versus vegetated land, that perpetuates the droughts. Like over Africa, an enhancement of tropical rainfall equatorward of these areas accompanies the summer drought. However, since winter heating of the land is minimal, regardless of the vegetation, and since Asia and Australia are not flanked by corresponding desertified land areas on the opposite side of the equator, there is no mechanism to enhance tropical low-level convergence during local winter so precipitation does not decrease during the dry season. Also, Asia and Australia are somewhat more influenced by mid-latitude storms during winter than the southern flank of the Sahara or South Africa. Precipitation driven by baroclinic instability is relatively insensitive to changes in boundary conditions.

The desert regions in the Americas have the weakest response. These areas are somewhat smaller, and have a more meridional than zonal orientation. Consequently, they do not impact the regional Hadley circulation as strongly as the other regions. The regions in

western North and South America have weak, localized monsoons which are not evident when the entire area of desertification is taken into account. These areas are also montane, and extend into mid latitudes where the abundance of baroclinic weather systems reduces the importance of vegetation change on climate. The Altiplano of Bolivia does show signs of increased summer drought like in the desertified regions of the eastern hemisphere. The Nordeste region of Brazil is the smallest of the desertified regions in this study. There is some indication of a decrease in precipitation during the wet season, but the anomalies are sporadic in sign and magnitude throughout the year, and not statistically significant.

This study shows that there is not a uniform response of climate to deforestation in all semi-arid parts of the globe. Local land–sea geometry, along with other topographical variations, contribute to unique responses to large-scale desertification in each region. It appears that for this GCM, the response can be categorized based upon the type and strength of the monsoon circulation. If this relationship can be shown to hold for more thorough simulations with higher spatial resolution and realistic boundary conditions, it might offer a first-order predictor for regional climate response to anthropogenic and natural changes in vegetation.

Acknowledgements

This research was supported by National Science Foundation grant ATM-93-41271, with computational support from the Scientific Computing Division of the National Center for Atmospheric Research. All figures were prepared using the Grid Analysis and Display System.

References

Allan, R. J. and Haylock, M. R. 1993 Circulation features associated with the winter rainfall decrease in southwestern Australia. *J. Climate*, **6,** 1356–1367

Bolin, B., Döös, B. R., Jager, J. and Warrick, R. A. 1986 *The greenhouse effect, climate change and ecosystems*. Wiley and Sons, New York

Bryson, R. A. and Lowery, W. P. 1955 Synoptic climatology of the Arizona summer precipitation singularity. *Bull. Am. Meteorol. Soc.*, **36,** 329–339

Charney, J. G. 1975 Dynamics of deserts and drought in the Sahel. *Q. J. R. Meteorol. Soc.*, **101,** 193–202

Charney, J. G., Quirk, W. J., Chow, S. H. and Kornfield, J. 1977 A comparative study of the effects of albedo change on drought in semi-arid regions. *J. Atmos. Sci.*, **34,** 1366–1385

Chervin, R. M. 1979 'Response of the NCAR general circulation model to changed land surface albedo'. Report of the JOC study conference on climate models: Performance, intercomparison and sensitivity studies, Washington, D.C., GARP Publ. Series, No. 22, Vol 1, 563–581

Davies, R. 1982 'Documentation of the solar radiation parameterization in the GLAS climate model'. NASA Tech. Memo 83961. Goddard Space Flight Center, Greenbelt, Maryland, USA

Delsol, F., Miyakoda, K. and Clarke, R. H. 1971 Parametrized processes in the surface boundary layer of an atmospheric circulation model. *Q. J. R. Meteorol. Soc.*, **97,** 181–208

Dickinson, R. E. 1983 Land surface processes and climate-surface albedos and energy balance. Pp. 305–353 in *Advances in geophysics*, Vol. 25, Academic Press

Dickinson, R. E. and Hanson, B. 1984 Vegetation–albedo feedbacks. Pp. 180–186 in *Climate processes and climate sensitivity. Geophysical Monograph* 29, *Maurice Ewing Volume* 5. American Geophysical Union

Dirmeyer, P. A. 1992 'GCM studies of the influence of vegetation on the general circulation'. PhD Dissertation. (Available from University of Maryland, College Park, MD 20742, USA)

Dorman, J. L. and Sellers, P. J. 1989 A global climatology of albedo, roughness length and stomatal resistance for atmospheric general circulation models as represented by the simple biosphere model (SiB). *J. Appl. Meteorol.*, **28,** 834–855

Douglas, M. W., Maddox, R. A., Howard, K. and Reyes, S. 1993 The Mexican monsoon. *J. Climate*, **6,** 1665–1677

Dregne, H. E. 1983 Desertification of arid lands. *Advances in desert and arid land technology and development, Volume* 3. Harwood Academic, New York

Graetz, D. 1994 Changes in land use and land cover: Grasslands. Pp. 125–148 in *Changes in land use and land cover: a global perspective.* Eds. W. B. Meyer and B. L. Turner. Cambridge University Press

Halpern, S. L. 1993 'The United Nations conference on environment and development: Process and documentation'. Academic Council on the United Nations System Reports and Papers 1993 No. 2, Providence, RI

Harshvardhan and Corsetti, T. G. 1984 'Longwave radiation parameterization for the UCLA/GLAS GCM'. NASA Tech. Memo 86072. Goddard Space Flight Center, Greenbelt, Maryland, USA

Harshvardhan, Davies, R., Randall, D. A. and Corsetti, T. G. 1987 A fast radiation parameterization for general circulation models. *J. Geophys. Res.*, **92,** 1009–1016

Hastenrath, S. and Greischar, L. 1993 Further work on the prediction of northeast Brazil rainfall anomalies. *J. Climate*, **6,** 743–758

Hou, Y.-T. 1990 'Cloud–radiation–dynamics interaction'. PhD Dissertation. (Available from University of Maryland, College Park, MD 20742, USA)

Janowiak, J. E. and Arkin, P. A. 1991 Rainfall variations in the tropics during 1986–89, as estimated from cloud-top temperatures. *J. Geophys. Res.*, **96,** 3359–3373

Kinter, J. L., Shukla, J., Marx, L. and Schneider, E. K. 1988 A simulation of the winter and summer circulations with the NMC global circulation model. *J. Atmos. Sci.*, **45,** 2486–2522

Kuo, H. L. 1965 On the formation and intensification of tropical cyclones through latent heat release by cumulus convection. *J. Atmos. Sci.*, **22,** 40–63

Lacis, A. A. and Hansen, J. E. 1974 A parameterization for the absorption of solar radiation in the Earth's atmosphere. *J. Atmos. Sci.*, **31,** 118–133

Lamb, P. J. and Peppler, R. A. 1992 Further case studies of tropical Atlantic surface atmospheric and oceanic patterns associated with sub-Saharan drought. *J. Climate*, **5,** 476–488

Laval, K. and Picon, L. 1986 Effect of a change of the surface albedo of the Sahel on climate. *J. Atmos. Sci.*, **43,** 2418–2429

Mabutt, J. A. 1984 A new global assessment of the status and trends of desertification. *Environ. Conserv.*, **11,** 103–113

Manabe, S., Wetherald, R. T. and Stouffer, R. J. 1981 Summer dryness due to an increase of atmospheric CO_2 concentration. *Clim. Change*, **3,** 347–386

Manabe, S., Spelman, M. J. and Stouffer, R. J. 1992 Transient responses of a coupled ocean–atmosphere model to gradual changes of atmospheric CO_2. Part II: Seasonal response. *J. Climate*, **5,** 105–126

McNeill, J., Alves, D., Arizpe, L., Bykova, O., Galvin, K., Kelmelis, J., Migot-Adholla, S., Morrisette, P., Moss, R., Richards, J., Riebsame, W., Sadowski, F., Sanderson, S., Skole, D., Tarr, J., Williams, M., Yadav, S. and Young, S. 1994 'Toward a typology and regionalization of land-cover and land-use change: Report of working group B'. Pp. 55–72 in *Changes in land use and land cover: A global perspective.* Eds. W. B. Meyer and B. L. Turner. Cambridge University Press

Meehl, G. A. 1992 Effect of tropical topography on global climate. *Annu. Rev. Earth Planet. Sci.*, **20,** 85–112

1994 Influence of the land surface in the Asian summer monsoon: External conditions versus internal feedbacks. *J. Climate*, **7,** 1033–1049

Mellor, G. L. and Yamada, T. 1982 Development of a turbulence closure model for geophysical fluid problems. *Rev. Geophys. Space Phys.*, **20,** 851–875

Mintz, Y.	1984	The sensitivity of numerically simulated climates to land-surface boundary conditions. Pp. 79–105 in *The global climate*. Ed. J. Houghton. Cambridge University Press
Miyakoda, K. and Sirutis, J.	1986	'Manual of the E-physics'. (Available from the authors at the Geophysical Fluid Dynamics Laboratory, Princeton University, P.O. Box 308, Princeton, NJ 08542 USA)
Moura, A. D. and Shukla, J.	1981	On the dynamics of droughts in northeast Brazil: Observations, theory and numerical experiments with a general circulation model. *J. Atmos. Sci.*, **38,** 2653–2675
Murakami, T.	1987	Orography and monsoons. Pp. 331–364 in *Monsoons*. Eds. J. S. Fein and P. L. Stevens. Wiley and Sons, New York
Namias, J.	1959	Persistence of mid-tropospheric circulations between adjacent months and seasons. Pp. 240–248 in *The atmosphere and the sea in motion*. Ed. B. Bolin. Rossby Memorial Volume
	1960	'Factors in the initiation, perpetuation and termination of drought'. Pp. 81–94 in Publication No. 51, I.A.S.H. Commission of Surface Waters
Nicholson, S. E.	1979	Revised rainfall series for the West African subtropics. *Mon. Weather Rev.*, **107,** 620–623
	1986	The spatial coherence of African rainfall anomalies; interhemispheric teleconnections. *J. Climate Appl. Meteorol.*, **25,** 1365–1381
Nobre, C. A., Sellers, P. J. and Shukla, J.	1991	Amazonian deforestation and regional climate change. *J. Climate*, **4,** 957–988
Oglesby, R. J. and Erickson III, D. J.	1989	Soil moisture and persistence of North American drought. *J. Climate*, **2,** 1362–1380
Pittock, A. B.	1983	Recent climate change in Australia: Implications for a CO_2 warmed earth. *Clim. Change*, **5,** 321–340
Rind, D.	1982	The influence of ground moisture conditions in North America on summer climate as modeled in the GISS GCM. *Mon. Weather Rev.*, **110,** 1487–1494
Ropelewski, C. F., Janowiak, J. E. and Halpert, M. F.	1985	The analysis and display of real time surface climate data. *Mon. Weather Rev.*, **113,** 1101–1107
Schneider, E. K. and Kinter III, J. L.	1994	An examination of internally generated variability in long climate simulations. *Clim. Dyn.*, **10,** 181–204
Schwartz, M. D. and Karl, Y. R.	1990	Spring phrenology: Nature's experiment to detect the effect of 'green-up' on surface maximum temperatures. *Mon. Weather Rev.*, **118,** 883–890
Sela, J. G.	1980	Spectral modeling at the National Meteorological Center. *Mon. Weather Rev.*, **108,** 1279–1292
Sellers, P. J., Mintz, Y, Sud, Y. C. and Dalcher, A.	1986	A simple biosphere model (SiB) for use within general circulation models. *J. Atmos. Sci.*, **43,** 505–531
Shukla, J. and Mintz, Y.	1982	Influence of land-surface evapotranspiration on the earth's climate. *Science*, **215,** 1498–1501
Skoupy, J.	1987	'Desertification in Africa. Agricultural and meteorological programs'. Pp. 33–45 in Proceedings of the Regional training seminar on drought and desertification in Africa, Addis Ababa. World Meteorological Organization
Slingo, J. M.	1987	The development and verification of a cloud prediction scheme for the ECMWF model. *Q. J. R. Meteorol. Soc.*, **103,** 29–43
Slutz, R. J., Lubker, S. J., Hiscox, J. D., Woodruff, S. D., Jenne, R. L., Joseph, D. H., Streurer, P. M. and Elms, J. D.	1985	'COADS: Comprehensive Ocean–Atmosphere Data Set. Release 1'. (Available from Climate Research Program, Environmental Research Laboratories, 325 Broadway, Boulder, CO 80303 USA)
Spencer, R. W.	1993	Global oceanic precipitation from the MSU during 1979–91 and comparisons to other climatologies. *J. Climate*, **6,** 1301–1326
Sud, Y. C. and Fennessy, M.	1982	A study of the influence of surface albedo on July circulation in semi-arid regions using the GLAS GCM. *J. Climatol.*, **2,** 105–125
	1984	Influence of evaporation in semi-arid regions on the July circulation: A numerical study. *J. Climatol.*, **4,** 383–398
Sud, Y. C. and Molod, A.	1988	A GCM simulation study of the influence of Saharan evapotranspiration and surface-albedo anomalies on July circulation and rainfall. *Mon. Weather Rev.*, **116,** 2388–2400
Sud, Y. C. and Smith, W. E.	1985a	Influence of local land-surface processes on the Indian monsoon: A numerical study. *J. Clim. Appl. Meteorol.*, **24,** 1015–1036

Sud, Y. C. and Smith, W. E.	1985b	The influence of surface roughness of deserts on July circulation (a numerical study). *Boundary-Layer Meteorol.*, **33,** 15–49
Sud, Y. C., Shukla, J. and Mintz, Y.	1988	Influence of land surface roughness on atmospheric circulation and precipitation: A sensitivity study with a general circulation model. *J. Appl. Meteorol.*, **27,** 1036–1054
Tiedtke, M.	1984	The effect of penetrative cumulus convection on the large scale flow in a general circulation model. *Beitr. Phys. Atmos.*, **57,** 216–239
Washington, W. M. and Meehl, G. A.	1984	Seasonal cycle experiment on the climate sensitivity due to a doubling of CO_2 with an atmospheric general circulation model coupled to a simple mixed-layer ocean model. *J. Geophys. Res.*, **89,** 9473–9503
Williams, M.	1990	Forests. Pp. 179–201 in *The Earth as transformed by human action: global and regional changes in the biosphere over the past 300 years*. Eds. B. L. Turner, W. C. Clark, R. W. Kates, J. F. Richards, J. T. Matthews and W. B. Meyer. Cambridge University Press, New York
	1994	Changes in land use and land cover: forests and tree cover. Pp. 97–124 in *Changes in land use and land cover: a global perspective*. Eds. W. B. Meyer and B. L. Turner. Cambridge University Press
Willmott, C. J., Rowe, C. M. and Mintz, Y.	1985	Climatology of the terrestrial seasonal water cycle. *J. Climatol.*, **5,** 589–606
World Resources Institute	1992	*World resources: 1992–1993*. Oxford University Press, New York
Xue, Y. and Shukla, J.	1993	The influence of land surface properties on Sahel climate: Part I: Desertification. *J. Climate*, **6,** 2232–2245
	1995	The influence of land surface properties on Sahel climate. Part 2: Afforestation. *J. Climate*, (in press)
Xue, Y., Sellers, P. J., Kinter, J. L. and Shukla, J.	1991	A simplified biosphere model for global climate studies. *J. Climate*, **4,** 345–364
Yanai, M. and Li, C.	1994	Mechanism of heating and the boundary layer over the Tibetan plateau. *Mon. Weather Rev.*, **122,** 305–323
Young, J. A.	1987	Physics of monsoons: The current view. Pp. 211–243 in *Monsoons*. Eds. J. S. Fein and P. L. Stevens. Wiley and Sons, New York